Final Report

Project Title:	Understanding the Effect of Na in Improving the Performance of $CuInSe_2$ Based Photovoltaics
Project Period:	09/01/2011 – 8/30/2015
Project Budget:	$960,000
Submission Date:	11/17 /15
Recipient:	University of Delaware
Address:	210 Hullihen Hall Newark, DE 19716-4602
Award Number:	DE-EE0005402
Project Team:	University of Illinois
Contacts:	Kevin Dobson Associate Scientist Phone: 302-831-6260 Email: kdobson@udel.edu

EXECUTIVE SUMMARY:

$Cu(In,Ga)Se_2$ (CIGS) thin film photovoltaic technology is in the early stages of commercialization with an annual manufacturing capacity over 1 GW and has demonstrated the highest module efficiency of any of the thin film technologies. However there still is a lack of fundamental understanding of the relationship between the material properties and solar cell device operation. It is well known that the incorporation of a small amount of Na into the CIGS film during processing is essential for high efficiency devices. However, there are conflicting explanations for how Na behaves at the atomic scale. This report investigates how Na is incorporated into the CIGS device structure and evaluates the diffusion of Na into CIGS grain boundaries (GBs) and bulk crystallites.

Participants: This project was carried out at the Institute of Energy Conversion (IEC) at the University of Delaware, collaborating with the Rockett group at the University of Illinois Urbana-Champagne (UI). Table 1 lists the participants involved in this project. Erten Eser retired in July 2014 and Kevin Dobson assumed PI responsibilities. Many aspects of this project culminated in the preparation of Robert Forest's Ph.D. thesis,[1] which he successfully defended in May 2015.

Table 1: List of project participants with their affiliations and project roles.

Participant	Affiliation	Role
Erten Eser	IEC	PI
Kevin Dobson	IEC	PI
Robert Forest	IEC	Grad. student
Robert Birkmire	IEC	Consultant
Brian McCandless	IEC	Consultant
Kunhee Han	IEC	Postdoc.
Angus Rockett	UI	Subcontract. PI
Xioqing He	UI	Postdoc.

Significant Findings: The significant outcomes of this project for each task include;

Task 1.0: Effect of Na in Devices Fabricated on PVD Deposited CIGS.

- Na diffusion occurs through the Mo back contact via GBs driven by the presence of oxygen,[2]

[1] R. V. Forest (2015) '*Diffusion of Sodium In Copper Indium Gallium Diselenide Based Materials'*, Ph.D. Dissertation, University of Delaware.

[2] R. V. Forest, E. Eser, B. E. McCandless, R. W. Birkmire and J. G. Chen, *AICHE Journal,* 60 (2014) 2365-2372.

- Na reversibly compensates donor defects in CIGS GBs,[3-5]

Task 2.0: Na Incorporation in Single Crystal CIGS

- bulk Na diffusion proceeds rapidly such that grains are Na-saturated immediately following CIGS thin film manufacture.[6]

Industry Guidance: The presented results offer interesting concepts for modification of manufacturing processes of CIGS-based PV modules. Possible approaches to improve control of Na uptake and uniformly increase levels in CIGS films are highlighted for processes that employ either soda-lime glass or NaF as the Na source. Concepts include the potential of O_2 or oxidative based treatments of Mo back contacts to improve Na diffusion through the metal film and increase Na uptake into the growing CIGS. This project has also offered fundamental understanding of the behavior of Na in CIGS grains and GBs, particularly the confirmation that CIGS grains will be saturated with Na immediately following manufacture

Summary of Results: Most commercially available CIGS modules are fabricated on soda-lime glass coated with Mo as the back electric contact, and Na in the glass diffuses through the Mo layer into the CIGS during film growth. In Task 1 the transport of Na through Mo was evaluated using x-ray photoelectron surface spectroscopy along with diffusion modeling to obtain diffusion coefficients at several temperatures. It was determined that Na diffusion in Mo only occurs along GBs and that oxygen provides an additional driving force to enhance Na transport. Device data revealed that older Mo substrates with a greater amount of surface oxide resulted in slightly higher efficiencies due to enhanced Na incorporation caused by the oxide. This finding shows that Mo substrates could potentially undergo an oxidation treatment prior to CIGS deposition to further improve and control the incorporation of Na.

To determine if in-grain Na affects device performance, in Task 1 Na was selectively removed from GBs using heat/rinse cycles. Due to the low temperature of this treatment, Na at GBS remained mobile while diffusion within the bulk was too slow for Na removal from the grain interiors. Changes in electrical properties were evaluated using conductivity and Seebeck coefficient measurements, with both decreasing as Na was removed to reach values similar to Na-free controls samples. This can be explained by the compensation of donor defects by Na, causing an increase in the free carrier concentration. Devices showed a decrease in open-circuit voltage after Na removal confirming that the beneficial effects of GB Na. The findings of this project will provide

[3] R. V Forest, K. Han, E. Eser, J. G. Chen and R. W. Birkmire, in *Proceedings of the 39th IEEE Photovoltaic Specialists Conference*, Tampa (2013).
[4] R. V. Forest, E. Eser, B. E. McCandless, J. G. Chen and R.W. Birkmire, in *Proceedings of the 40th IEEE Photovoltaic Specialists Conference*, Denver (2014).
[5] R. V. Forest, E. Eser, B. E. McCandless, J. G. Chen and R. W. Birkmire, *J. Appl. Phys.* 117 (2015) 115102.
[6] R. V. Forest, B. E. McCandless, X. He, A. A. Rockett, E. Eser, K. D. Dobson, R. W. Birkmire, (2015) submitted to *Adv. Mater*.

guidance for rational optimization of Na incorporation procedures in the manufacturing of CIGS solar cells.

While it is known that Na segregates at CIGS GBs, the nature and role of Na diffusion into grain interiors was less clear. In Task 2, single crystal $CuInSe_2$ was used as a model system to represent the grain interiors of CIGS. Crystals processed by two different methods of different compositions and dislocation densities, were evaluated. Diffusion coefficients were obtained at two temperatures after Na diffusion, giving near identical values, ~$2x10^{11}$ cm^2/s and ~$6x10^{11}$ cm^2/s at 420°C and 480°C, respectively, for each crystal. Characterization confirmed that dislocation densities were too low to significantly impact the effective diffusion coefficient. The Cu-poor crystal had a higher solubility suggesting that Na diffusion is mediated by Cu-vacancies, but was not accompanied by an expected increase in diffusion coefficient. The activation energy for diffusion was similar to values expected for interstitial diffusion, but the large size of Na^+ ions should result in a solubility that is much lower than what was experimentally measured. A hybrid interstitial-substitutional mechanism is proposed that combines the fast diffusion of interstitial atoms with the high solubility common for substitutional impurities. Lattice diffusion of Na proceeds fast enough that CIGS grain interiors will have Na concentrations near the solubility limit of 10^{18} cm^{-3} when manufactured under standard conditions. Na and K treated epitaxial CIS films showed a significant increase in cathodoluminescence emission intensity, indicating a reduction of non-radiative recombination pathways, which is consistent with improvements in CIGS device performance, though the mechanism is not clear.

While preliminary results were comparable to those obtained under Task 1, efforts under *Task 3. Effect of Na in Devices Fabricated on CIGS Processed by Precursor Selenization* were not fully pursued due to delays as a result of major upgrades to the selenization reactor at IEC and the subsequent high usage of the system by other groups and projects. The studies of Na diffusion in single crystal under Task 2 were found to be a very rich source of significant results and continued efforts under Task 3 were abandoned.

Pathways forward: Despite the success of this project, there are a number of questions remaining related to further the understanding of the chemistry of Na in CIGS films and devices. These include further elucidation of the mechanisms of Na passivation in CIGS GBs, with identification of which defects are involved and confirmation of the possible effects of in-grain Na on device performance. To complete analysis of the cell structure, conformation of the presence and possible chemistries of Na at the CIGS/CdS junction and/or in the front transparent contacts, and its effects on device performance, is needed.

TABLE OF CONTENTS

BACKGROUND:

A crucial aspect in the manufacturing of $Cu(In,Ga)Se_2$ (CIGS) solar cells is the introduction of a small amount of Na into the CIGS absorber layer. It is well known that a Na concentration on the order of 1×10^{19} atoms/cm^3 will increase both device open circuit voltage (V_{oc}) and fill factor (FF) [1-5]. Incorporation of Na can lead to a relative increase in efficiency as high as 60% [6] and is necessary for manufacture of high efficiency and cost-effective modules.

Na can be incorporated using a wide variety of techniques. The simplest and most widely used method is to use a soda-lime glass (SLG) substrate as a Na source. SLG contains ~14 wt% Na_2O, and with the high temperatures used during the CIGS deposition, Na becomes mobile and diffuses through the Mo layer into the growing CIGS film. This incorporation method is simple and inexpensive, though it can result in non-uniform Na concentrations [7]. An external source of Na ions can be used instead of relying on Na from the substrate. Earlier studies used Na_2Se [3,8-12], but NaF is now more common because it is less hygroscopic, easier to handle, and gives the same improvements in performance. An external Na source also allows the use of Na-free substrates, such as flexible metal foils. If SLG is used along with an external Na source, an alkali diffusion barrier such as Al_2O_3 or SiO_2 is often deposited on SLG to prevent Na diffusion [5,13] as large amounts of Na can be detrimental to device performance [3,14-17].

Na compounds can be added before [3,5,18-20], during [9-13,16,21,22] or after CIGS deposition [13,16,23,24], all with similar increases in efficiency. Na incorporation before CIGS deposition involves depositing a Na-precursor layer on either the substrate or Mo, though this can cause adhesion problems if the layer is too thick. An alternative is to incorporate Na during the Mo deposition by doping the Mo sputter target with Na [25-29]. Deposition of Na compounds during the CIGS deposition is commonly referred to as co-evaporation, and the exact time at which Na is added can alter electrical properties [16]. Na deposition after CIGS is known as a post deposition treatment (PDT).

Na has been attributed with a number of changes to CIGS such as the formation of larger grains [7], preferential orientation of grains [30], increased p-type conductivity [19], and inhibition of In/Ga interdiffusion [31]. It is unclear if the effects of Na are due to a single mechanism or from several beneficial effects. However, since the low temperatures used during NaF PDT cannot alter the CIGS grain structure, effects that require Na during growth, such as an increase in grain size with Na, cannot be the primary mechanism for improving CIGS [6]. Therefore, this report focuses on the non-structural effects of Na.

Historically it has not been clear if Na effects are due to its presence at grain boundaries or within grain interiors. It has long been established that Na in CIGS segregates at grain boundaries (GBs) [32] , but recent atom-probe tomography (APT) measurements reveal that a small amount of Na diffuses into the bulk reaching concentrations up to 100 ppm [33]. At these concentrations, Na has the potential to impact device performance. However, it is still not known if Na within grain interiors plays an active

role in improving device performance, and this issue was one of our key focuses.

INTRODUCTION:

It has been shown that Na, supplied by out-diffusion from SLG through the Mo back contact greatly improves the performance of CIGS devices. However, out-diffusion from the glass is too poorly controlled to provide adequate process yields. The basic effects of Na on CIGS itself have been known for some time. It is not a dopant in CIGS but shows some evidence of reduction of compensating donor density in the films. It has been also suggested that Na passivates the GBs, though proposed models are not verified experimentally. A fundamental understanding of the pathways of the effects of Na is needed, along with confirmation of the optimum incorporation method and necessary Na concentration levels for different CIGS thin film processing.

The proposed project had two objectives, i) to find the pathways through which Na improves CIGS device performance and ii) to demonstrate a Na incorporation scheme that gives equivalent performance levels on different substrates from CIGS films deposited in prototype manufacturing tools, such as roll-to-roll physical vapor deposition (PVD) and precursor selenization. This project addressed such issues as determine the diffusion mechanism of Na in Mo back contact films in polycrystalline CIGS, the level of Na incorporation in CIGS grain interiors, and determining the mechanism and role of defects in the observed beneficial Na effects.

The project scope consisted of four tasks over two budget phases. These tasks with milestones are listed below.

Task 1.0: Effect of Na in Devices Fabricated on PVD Deposited CIGS.

Subtask 1.1: Na Incorporation by Diffusion from SLG Substrates in Vapor Deposited CIGS

- Determine grain structure, crystallography and Na distribution for CIGS films.
- Fabricate and characterize devices.

Subtask 1.2: Na Incorporation by Post-Deposition of NaF on Vapor Deposited CIGS and in-situ Annealing

- Determine grain structure, crystallography and Na distribution.
- Fabricate and characterize devices

Subtask 1.3: Na Incorporation from NaF Co-Evaporation During CIGS Deposition

- Determine grain structure, crystallography and Na distribution at nano and macro level.
- Fabricate and characterize devices.

Task 2.0: Na Incorporation in Single Crystal CIGS

Subtask 2.1: Growth of Na Doped Epitaxial Layers

- Growth of Na doped epitaxial layers with experimental data on Na incorporation from NaF source.

Go/No Decision point.

- Determine Na incorporation into CIS and CIGS single crystal epitaxial layers within the temperature range (450 to 550 C) used for the deposition of PV quality CIS and CIGS thin films. Such epi-layers will have Cu-to-group III ratios between 0.95 to 0.85, similar to PV quality thin films. Similarly, CIGS alloy samples will be studied. The minimum expectation is coverage of one alloy composition between 10 and 50% Ga/In+Ga, along with the Ga-free epi-layer as the control. Achievement of a Ga-to-group III ratio between 0.25 to 0.35 will be a bonus because this covers the composition range of typical devices. Na incorporation should not result in second phases and preserve the original single crystal structure. The amount of Na will be determined by SIMS or other appropriate measurement techniques, and its electronic effect will be determined by comparing electronic properties and if necessary by comparing device characteristics of the doped and un-doped epi-layers.
- Experimental picture of how Na influences evaporated CIGS device performance when diffused from substrate or co-evaporated.

Subtask 2.1: Growth of Na Doped Epitaxial Layers

- Complete studies of the growth of CIGS in the presence of NaF showing how addition of NaF leads to incorporation of Na into bulk CIGS single crystals under different processes such as ex-situ doping by thermal annealing, using other Na source materials.

Subtask 2.2: Effect of Oxygen on Na Doped Epitaxial Layers

- Determine the pathways for oxygen incorporation into the epitaxial CIGS.
- Understanding of how oxygen affects material characteristics of the epitaxial layers and how it controls Na incorporation.

Subtask 2.3: Effect of Na on Devices Produced from Epitaxial CIGS

- Fabrication, characterization and modeling of solar cells produced from single crystal epitaxial CIGS layers of different composition from subtasks 2.1 and 2.2.

Task 3. Effect of Na in Devices Fabricated on CIGS Processed by Precursor Selenization.

Subtask 3.1: Na Incorporation by Diffusion from SLG Substrates for CIGS Processed by Precursor Selenization

- Determine grain structure, crystallography and Na distribution at nano and macro level for both CIGS films grown to completion and the ones interrupted (quenched) before completion.
- Fabricate and characterize devices

Subtask 3.2: Na Incorporation from NaF Films Deposited on Precursors and Post-deposited on Selenized CIGS Films Followed by Annealing

- Determine grain structure, crystallography and Na distribution at nano and macro level for both CIGS films grown to completion and the ones interrupted before completion.
- Fabricate and characterize devices.

Task 4.0: Project Management and Reporting

- No milestones under this task.

Under Task 1, CIGS films deposited by elemental co-evaporation were studied on different substrates, determining the fundamentals of Na diffusion in Mo and CIGS. This included determining the role of oxygen and identifying mechanistic details. Oxygen levels were shown to affect Na GB diffusion in Mo, which suggests that Mo substrates could potentially undergo an oxidative treatment prior to CIGS deposition to help optimize Na incorporation. Electrical measurements, including conductivity and Seebeck coefficients, were used to elucidate the nature of Na diffusion and its fate in the CIGS films. A mechanism where Na compensates of donor defects in the GBs increasing free carrier concentration is suggested. Task 2 dealt with Na diffusion in CIS single crystals and single crystal epitaxial films (U. of Illinois), as a model for the CIGS grain interior. This allowed the identification of the in-grain Na diffusion mechanism and confirmed that grains in polycrystalline CIGS thin films will be Na-saturated when processed at standard manufacturing conditions. Na and K incorporation in epitaxial CIS films showed a significant increase in cathodoluminescence (CL) intensity, suggesting a reduction of non-radiative recombination pathways, which is consistent with improvements in CIGS device performance. Task 3 was to monitor the role of Na in CIGS manufactured by selenization of sputtered precursor metal films.

Many of the results presented in this report culminated in the preparation of Robert Forest's Ph.D. thesis, which he successfully defended in May 2015 [34].

PROJECT RESULTS AND DISCUSSION:

A. Task 1.0: Effect of Na in Devices Fabricated on PVD Deposited CIGS.

1. Sodium Diffusion Through the Mo Back Contact Layer

One of the simplest methods for incorporating Na is via diffusion from a SLG substrate through the thin Mo back contact layer during CIGS deposition. With the high temperatures during deposition, typically 450 - 600°C, Na diffuses through the Mo into the growing CIGS film. The amount of Na incorporated by this approach is not well controlled and can result in non-uniform distribution over large areas [7], however, it remains an attractive option due to its simplicity and low cost. Developing a better understanding of the Na diffusion mechanism through Mo films can lead to solutions to overcome this issue.

While there have been several studies on how the Mo back contact affects Na incorporation in CIGS [35- 41], the specific diffusion mechanism is not well understood. The current understanding is that, at CIGS deposition temperatures, Na is highly mobile along Mo GBs [39] but does not diffuse into the grain interiors, as Na solubility is negligible up to the Mo melting point [42]. Therefore, it is unlikely that any bulk transport takes place within the Mo grains. Since grains in a typical Mo back contact are columnar and span the entire height of the film [43], GBs provide a fast diffusion path to the CIGS interface. Near the Mo/CIGS interface, Na tends to segregate, and has been observed by different groups [38,41]. The amount of Na that accumulates at the Mo surface may determine how much is incorporated into the CIGS film.

The void fraction or porosity of the Mo film also has a large effect on Na levels incorporated into CIGS films [35-38,42], with less Na is observed in films grown on dense Mo compared to those grown on more porous Mo. It is believed that these voids occur along GBs and store oxygen, which is known to facilitate Na diffusion [38,39]. Previous work in our group has shown that Na does not accumulate on the Mo surface when heating under high vacuum in the absence of oxygen [44]. CIGS deposited on intentionally oxidized Mo has been shown to have higher Na concentrations [38], and CIGS devices made on oxidized Mo show a small improvement in open circuit voltage (V_{OC}) and fill factor (FF), likely due to higher Na levels [45].

The role that oxygen plays on the accumulation of Na on the Mo film surface was investigated this project. Specifically, we show that at a given temperature, less Na accumulates on the Mo surface if oxygen is removed prior to diffusion, and more if oxygen is added. Based on the experimental results, a diffusion model is used to explain Na diffusion from SLG and its accumulation on Mo. By fitting the model to diffusion data at different temperatures, the apparent activation energy (E_a) for GB diffusion of Na through Mo is determined.

Mo films, ~700 μm thick, were sputter-deposited on SLG substrates. The surface composition of the Mo films was analyzed using x-ray photoelectron spectroscopy (XPS). The XPS chamber was equipped with a differentially pumped ion gun for sputter

etching. The ion beam raster size was 1 x 1 cm^2, which covered the entire sample. Sample heating was performed using a Ta wire resistive heater in a separate process chamber attached to the XPS system through a gate valve. Samples could be transferred between the process and analysis chamber under vacuum and without air exposure.

Cross-sectional scanning electron microscope (SEM) images were used to characterize the grain structure of the Mo films, and the measured dimensions were used as input parameters for modeling Na diffusion through Mo. Figure 1a shows the SEM image of a 680 nm thick Mo film having columnar grains of 50 nm average width extending through the entire film. Figure 1b shows a simplified cross-sectional schematic of the Mo film with arrows denoting the diffusion path of Na. Figure 1c shows a schematic of a close up of a Mo grain boundary along with adjacent grains and denotes the dimensions that will be used in modeling the diffusion of Na.

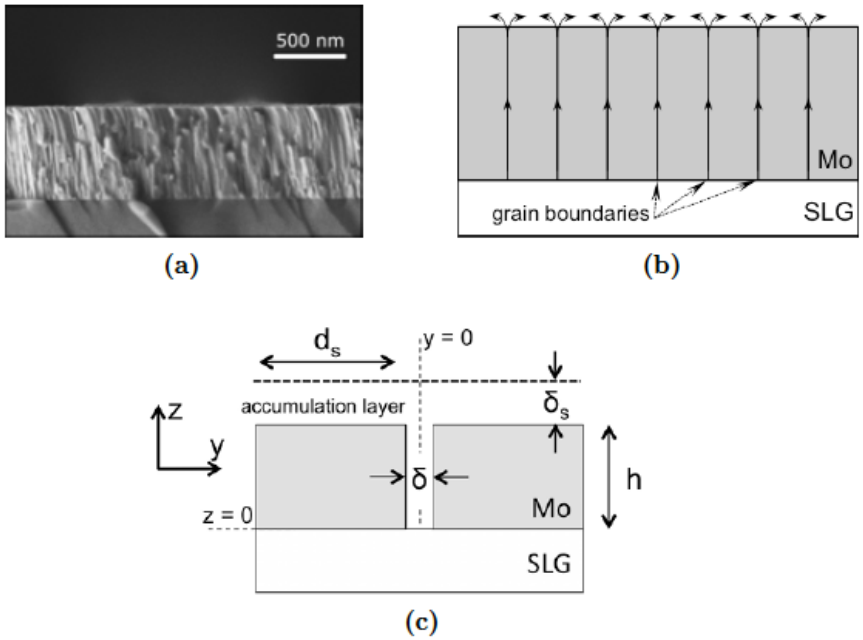

Figure 1: (a) Cross-section SEM image of sputter deposited Mo on SLG. (b) Enlarged schematic of seven Mo grains with arrows denoting the diffusion path of Na. (c) Schematic depicting two adjacent Mo grains with their shared GB. Dimensions used for diffusion modeling are not to scale

XPS measurements of the Mo 3d, O 1s, and Na 1s regions were obtained for the as-deposited Mo/SLG sample surface. Composition was determined to be 47 at% Mo and 53 at% O with no Na observed. The Mo 3d region of the spectrum is shown in Figure 2a and reveals that MoO_2, MoO_3, and metallic Mo are all present on the surface. For this particular sample, 82% of the measured Mo is metallic, 3% is MoO_2, and 15% is assigned to MoO_3. The peak areas of the Mo oxides are in good agreement with the

levels of measured oxygen. XPS depth profiling (Figure 3a) reveals that MoO_3 exists only with the first few nanometers of the film, while MoO_2 is detectable further into the film. Qualitative secondary ion mass spectroscopy (SIMS) measurements (Figure 3b) show that the oxygen level is nearly constant through the entire film, confirmed to be ~2 at% from Auger electron spectroscopy (AES) depth profiling. The oxygen likely originates from residual gas in the chamber during sputter deposition of the film. Given the very low solubility of O in Mo [46], most of the oxygen must reside in the GBs. After heating the Figure 2a sample for 10 min at 400°C, Na appeared in the spectrum at a concentration of 4 at% (Figure 2b). The Na 1s peak was located at 1072.5 eV, consistent with the binding energy of Na_2O.

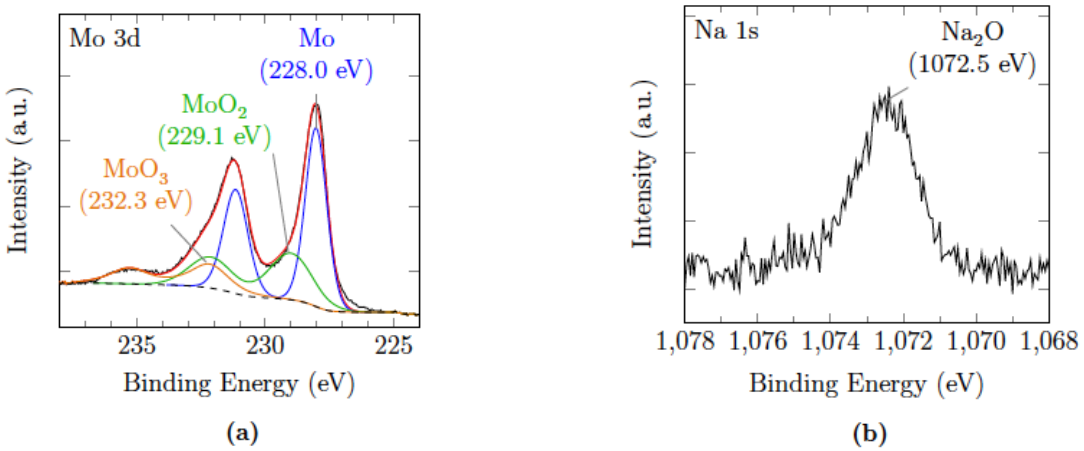

Figure 2: (a) XPS spectrum of Mo 3d region for as-deposited Mo surface showing peaks for oxide and metallic species. (b) XPS spectrum of Na 1s region for SLG/Mo sample after heating at 400°C for 10 min.

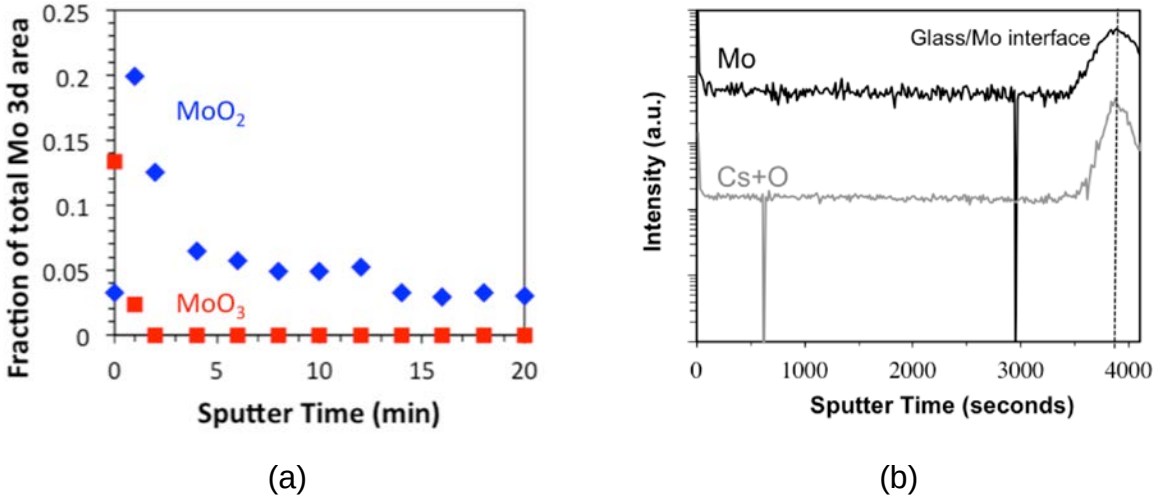

Figure 3: (a) XPS and (b) SIMS depth profiles through the surface of Mo/SLG.

To evaluate the relationship between oxygen levels and Na accumulation, the Mo

surface oxygen concentration was precisely controlled prior to diffusion by either sputtering in the XPS to remove oxygen or by heating in air to add oxygen. Heating the Mo/SLG samples in ambient air at 200°C for 30 min increased the surface oxygen content from roughly 50 at% for the as-deposited film to 65 at% (Figure 4a). Depth profiling measurements with XPS reveal that this oxide layer is only a few nanometers thick. It was determined that Na diffusion in Mo at this temperature is too slow to cause any significant diffusion of Na out of SLG during treatment. Figure 4b shows the decrease in surface oxygen with sputter etching time. The Mo thickness is reduced by <1% during sputtering and will have no affect on the diffusion measurements. The oxygen concentration stabilizes at an artificially high concentration after long periods of etching, likely due to a small amount of surface oxygen being pushed into the film during sputtering and preventing the complete removal of oxygen from the surface. Surface oxygen concentrations as low as 16 at% can, however, be achieved using this procedure. Diffusion experiments were performed immediately after etching without ambient air exposure to avoid re-oxidation of the Mo surface.

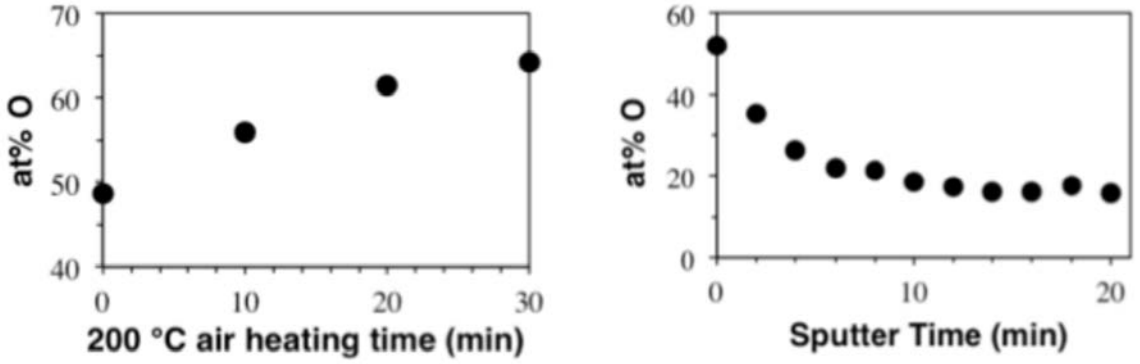

(a) (b)

Figure 4: Surface oxygen content of Mo films on SLG as measured by XPS for samples (a) heated in ambient air at 200°C and (b) sputter-etched in vacuum.

The accumulation of Na on SLG/Mo during heating in vacuum was compared between a sample having 53 at% surface oxygen due to ambient air exposure, and a sample with 16 at% surface oxygen following sputter-etching. These samples were both heated at 400°C in vacuum for 1 to 2 min at a time, cooled to near ambient temperature, then transferred to the XPS analysis chamber for surface Na measurement. This process was repeated on the same sample until the Na concentration had plateaued. Figure 5 shows results for both samples. Within 10 min total heating, the surfaces of both samples become Na saturated and concentration no longer increases with further treatment. The saturation concentration varies by nearly an order of magnitude between the samples, with the high oxygen sample showing a higher total Na accumulation of 4 at%, compared to 0.5 at% for the low oxygen piece. This indicates that Mo surface oxygen directly affects the amount of Na that can accumulate.

To clarify this relationship further, similar heat treatments were performed several Mo/SLG samples with surface oxygen concentration ranging from 27–59 at%. These samples were heated under vacuum at either 400°C or 500°C until the Na concentration saturated. In Figure 6 the Na saturation concentration is plotted against the amount of surface oxygen before heating. The figure shows a linear relationship at both temperatures where increasing Na levels are seen with higher surface oxygen, conforming the critical role O plays a in controlling Na saturation concentration on Mo. However, it is not clear why the saturation concentration is greater for samples that were heated to higher temperature.

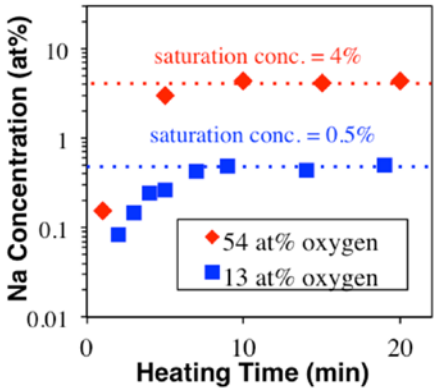

Figure 5: Na concentration on Mo surface as measured by XPS as a function of heating time at 400°C for samples with high (red diamonds) and low (blue squares) surface oxygen.

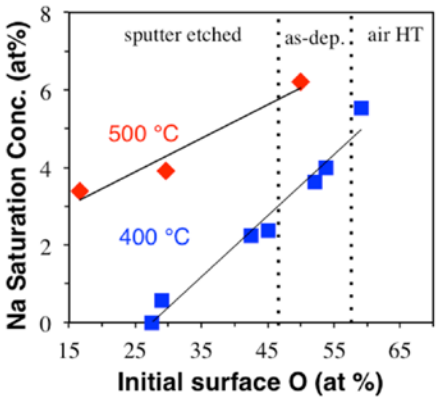

Figure 6: Na saturation concentration as a function of initial surface oxygen on Mo films after heating in vacuum at 400°C (blue squares) and 500°C (red diamonds).

Mathematical modeling was performed to explain the observed relationships and quantify the diffusion process. Na accumulation data was fit to a Hwang-Balluffi diffusion model [47] and Figure 7 shows best fits for Mo/SLG samples heated at 300°C, 350°C,

and 400°C. Table 2 shows the optimized GB diffusion coefficients (D_b) from these three temperatures and compares an as-deposited sample with a low oxygen sputter-etched sample following 400°C treatment. The optimized values of D_b at 400°C for both the as-deposited and sputter-etched samples vary by only 50%, which is not significant given the precision of these measurements. While oxygen at GBs plays a role in Na diffusion, sputter-etching does not alter the amount of oxygen through the majority of the film and, therefore, D_b would remain unchanged. It has been demonstrated that Na diffusion is enhanced in Mo films with greater bulk oxygen concentrations [38,48] and it is expected that the value of D_b would increase with higher GB oxygen levels.

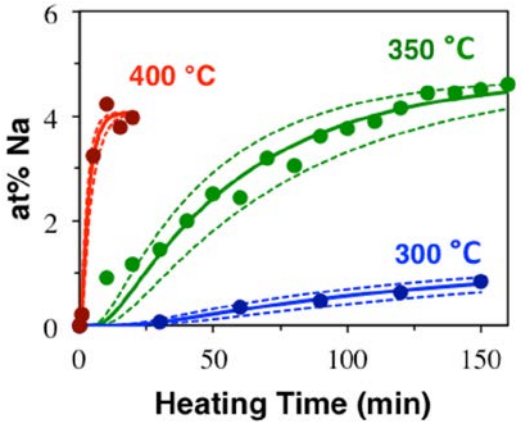

Figure 7**:** The Hwang-Balluffi model (solid line) fit to experimental data (circles) for as-deposited SLG/Mo samples after diffusion at 400°C, 350°C, and 300°C. Dashed lines denote the model with ± 25% of the optimized GB diffusion coefficient.

Table 2: Optimized values of D_b for Na in thin film Mo at various temperatures and surface oxygen levels.

Treatment	Initial O (at %)	T (°C)	D_b (cm^2/s)
Sputter-etched	11	400	7.8×10^{-12}
None	53	400	12×10^{-12}
None	44	350	6.5×10^{-13}
None	54	300	2.9×10^{-13}

As expected D_b increases with temperature. Typically the temperature dependence of a diffusion coefficient follows an Arrhenius type relation:

$$D(T) = D_0 \exp\left(\frac{E_a}{RT}\right) \quad (1)$$

where D_0 is the pre-exponential factor. Figure 8 plots the natural logarithm of D_b against the inverse of temperature. The linear plot confirms that Na diffusion through Mo has an Arrhenius type dependency with temperature. The slope resulted in an estimate of the apparent E_a of 117 kJ/mol. As a rule of thumb for GB diffusion in metals, Gupta suggests that E_a in calorie/mol should be 17 to 25 times the melting temperature of the diffusion matrix in Kelvin [49]. For GB diffusion in Mo, this gives an estimated E_a of 200 to 300 kJ/mol. As the measured E_a is significantly lower than expected, it is likely that the transport of Na in Mo may not follow a standard mechanism for GB diffusion. However, Arnoldy et al. [50] report an E_a of Mo-O bond breaking during the reduction of MoO_3 of 120 kJ/mol, which is in excellent agreement with E_a from Figure 8. The similarity in E_a suggests that the M-O bond is potentially involved in the mechanism of Na GB diffusion in Mo thin films.

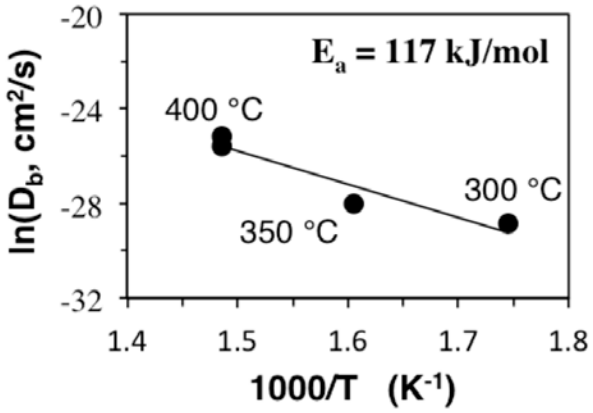

Figure 8: Arrhenius plot for the Na diffusion in Mo thin films.

Based on these results, it may be possible to enhance Na incorporation into CIGS by controlling the amount of surface oxygen on Mo substrates, increasing the diffusion rate so that higher levels are incorporated and improve device performance. However, due to the high temperatures during CIGS deposition, additional surface oxygen would only slightly improve Na incorporation levels. At a standard deposition temperature of 580°C, Na would diffuse through a 1 μm film in 15 s. At such a rapid diffusion rate, additional surface oxygen would only marginally enhance the Na incorporation. However, for manufacturing processes that involve sequential Mo and CIGS depositions without exposure to atmosphere, the absence of oxygen could make Na incorporation less favorable. Also, in processes with lower CIGS deposition temperatures, Na diffusion in Mo may become slow enough that Mo surface oxidation becomes a more significant factor.

Although Mo surface oxygen plays only a minor role in the incorporation of Na in CIGS at high deposition temperatures, the amount of surface oxidation can still be optimized to provide slight improvements in device V_{OC} and efficiency. An increase in efficiency with Mo age has been independently observed by Salomé et al. [45] providing more support to this hypothesis. The simplest approach to monitor such effects is to compare device performance against the age of the Mo/SLG substrates before CIGS deposition. Mo samples that remain in storage longer will have greater exposure to air and will accumulate more surface oxygen. Figure 9 shows data from the IEC cell performance database for 280 (Ag,Cu)(In,Ga)Se_2 (ACIGS) devices, plotting V_{OC} with Mo age. All samples had Ga/(In+Ga) = 0.47–0.53 and Ag/(Cu+Ag) = 0.2–0.4 to minimize the effects of composition on band gap and cell performance. Despite a few outliers from poor performing cells, the figure shows a slight performance improvement with Mo age, consistent with increasing surface Mo oxidation enhancing Na incorporation.

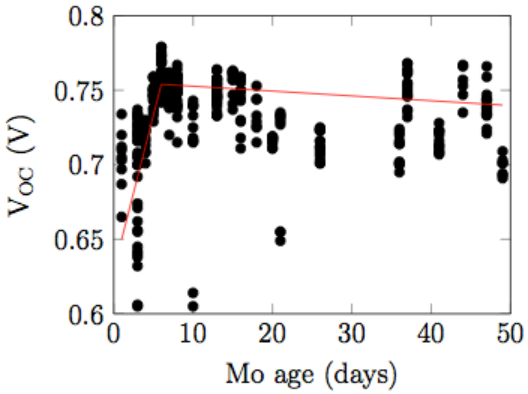

Figure 9: V_{OC} of ACIGS devices vs. age of Mo before ACIGS deposition. Line is to aid the eye.

These results raise the possibility that the Mo substrates could undergo a partial oxidation treatment to optimize the amount of surface oxide, though care must be taken not to provide excess oxygen as an overly oxidized surface would have several detrimental effects on device performance. MoO_3, in a thick surface oxide film, is an intercalation host for Na [51] due to its layered structure, and may act as Na sink preventing incorporation into CIGS. This is not an issue for low oxygen samples as sub-monolayer amounts of MoO_3 do not form the layered structure. Excess surface oxygen would also compete with the formation of $MoSe_2$, which is known to facilitate the formation of an ohmic back contact in CIGS devices [52]. Lastly, MoO_3 is not conductive and a thick oxide layer on the back contact would increase device series resistance.

The results related to Na diffusion in Mo back contact films were published during the project [53].

2. *Reversibility of ACIGS electrical properties*

The presence of Na increases p-type conductivity in CIGS [19, 54 - 56] and the mechanism for this is attributed to a variety of point defects. If Na occupies In or Ga sites, denoted as Na_{In} and Na_{Ga}, respectively, it will directly act as an acceptor, increasing the hole concentration [57]. Niles et al. reported evidence of Na bound to Se and attributed this to the substitution of Na into In sites [57]. However, density functional theory (DFT) computations disagreed whether this defect is energetically favorable [58,59,80]. An alternate hypothesis suggests Na replaces In_{Cu} defects to form Na_{Cu} [55,56]. Na_{Cu} does not introduce energy levels within the band gap and is electrically inactive [58]. However, the In_{Cu} defect is an electrically active donor and replacing it would lower the concentration of compensating electrons.

It is also possible that Na improves device performance by passivating GB defects. Both Mungan et. al. [60] and Urbaniak et. al. [61] provide models describing how the passivation of GBs can enhance cell performance. The removal of GB donor defects can increase carrier concentrations and reduce recombination traps near GBs. Cahen and Noufi suggest that the primary electrically active defect at GBs is the selenium vacancy (V_{Se}) [62], and Kronik et. al. present a model for V_{Se} passivation in which Na catalyzes the oxygenation of this defect to form electrically neutral O_{Se} [63]. A majority of Na in CIGS resides at GBs, supporting the GB passivation model, though small amounts of Na in grain interiors could still impact electronic properties (see later discussion). Rudmann et al. propose that Na does not affect grain interiors when incorporated with a NaF PDT because the lower temperatures used prevents Na diffusion into grains [6]. However, more recent APT measurements reveal the presence of small Na levels in CIGS grain interiors after NaF PDT [76] and, therefore, Na effects on the electronic properties of grain interiors cannot be ruled out.

The incorporation of Ag into CIGS to form (Ag,Cu)(In,Ga)Se_2 (ACIGS) has been of recent interest because of its ability to raise the band gap while lowering defect density, providing a pathway to higher efficiency devices [64]. ACIGS has the same chalcogenide structure as CIGS, with Ag substituting with Cu. The effect of Na is much less studied in ACIGS, but it is known to similarly increase V_{OC} and FF. Because of the similarities in structure, the same Na-related defects that improve CIGS are likely responsible for improvements in ACIGS.

In this project the effect of Na addition and removal on the electrical transport properties in ACIGS films was investigated. A novel procedure was developed that allowed Na to be cyclically removed and re-introduced into the film. A combination of conductivity and Seebeck coefficient measurements showed how Na affects electrical transport properties and the results are interpreted in terms of GB chemistry.

ACIGS films were deposited on 1 x 1 $inch^2$ alumina pieces (99.6% purity) to eliminate the substrate as a Na diffusion source. It was confirmed that the Na content of the substrates fell below detection limits of both XPS and energy-dispersive x-ray spectroscopy (EDS). To allow for device and electrical measurements on the same sample, the substrate was masked during the Mo deposition to give a 1 mm gap for

measuring conductivity and a 8 mm x 20 mm Mo-free area for measuring the Seebeck coefficient (Figure 10). ACIGS was deposited by three-stage coevaporation with a substrate temperature of 580°C with composition Ag/Cu+Ag = 0.26, Cu+Ag/In+Ga = 0.78, and Ga/In+Ga = 0.54. After deposition, 20 nm of NaF was deposited at room temperature by e-beam evaporation. After a brief exposure to air, the sample was transferred to a separate vacuum chamber where it was heated to 400°C for 20 minutes to induce Na diffusion into the ACIGS film. After cooling, the sample was rinsed in water to remove excess NaF from the surface. An identical alumina/ACIGS sample without NaF treatment was used as a Na-free control.

Na was removed from the ACIGS samples, as shown in the experimental flow chart in Figure 11, with multiple cycles of rinsing in DI water (18 Mohm-cm) at 60°C followed by heating in air at 200°C for 5-10 minutes. Na compounds are typically very soluble in water, and rinsing is expected to completely remove Na from the surface. XPS measurements verified that the surface Na concentration after rinsing was below the instrument detection limit of ~0.1 at%. The presence of oxygen increases the rate of Na diffusion and so heat treatments to accumulate Na on the film surface were carried out in air. The decrease in Na with the combination of surface accumulation and rinsing makes it possible to control Na content in the film with the number of heat/rinse cycles. The ACIGS samples underwent multiple rinse/heat cycles, with conductivity and Seebeck coefficients measured after each cycle. After 31 cumulative minutes of heating, to test the reversibility of Na treatments, NaF was re-deposited and the Na removal cycles and electrical measurements were repeated.

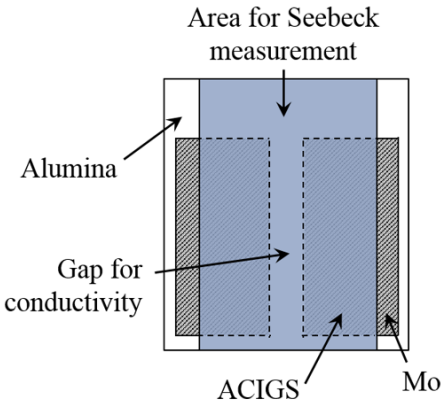

Figure 10: Schematic of Mo pattern used with ACIGS samples on alumina substrates for conductivity and Seebeck measurements.

The Na removal conditions were chosen so that Na would be specifically removed from GBs rather than from grain interiors. To significantly deplete Na from grain interiors, the diffusion length, $2\sqrt{Dt}$, must be larger than the width of the grain. At 31 minutes of heating, the bulk diffusion coefficient must be 1×10^{-12} cm^2/s to give a diffusion length of 1 µm, which is unrealistically large for lattice diffusion at 200°C and unlikely to deplete

the in-grain Na within 31 minutes. With the chosen benign conditions, the rate of Na diffusion out of the grain interiors would most likely be too slow to account for the large changes observed in electric properties, and, therefore, GB Na is being specifically removed from the films.

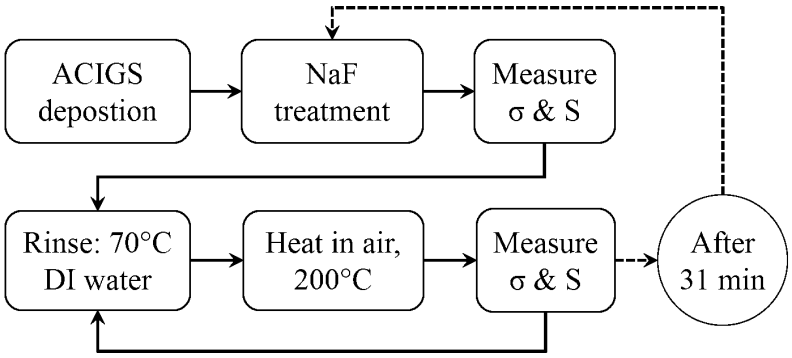

Figure 11: Flow diagram for the experimental procedure for Na removal.

Cross-grain conductivity (σ) of the ACIGS films was obtained from resistance measurements across the 1 mm gap in the Mo back contacts using a Kelvin probe setup in the dark at room temperature. Since σ is based on resistance measured across many grains, it is actually an effective conductivity based on contributions from both the grain interiors and GBs. Seebeck coefficients (S) were also monitored on these samples. The Seebeck effect is a thermoelectric phenomenon in which a voltage is induced by an applied thermal gradient. This voltage difference between two probes spaced 1 cm apart is measured using the setup shown in Figure 12. These probes are temperature controlled, so voltage is measured at the exact location that the temperature gradient is applied. One probe is a thermocouple embedded within a heating block that is held at 100°C, while the second is a spring loaded stainless steel tip held near room temperature. *S* is determined as the ratio between the measured voltage (V_{hot} - V_{cold}) and applied temperature difference, (T_{hot} - T_{cold}), where

$$S = -\frac{V_{hot} - V_{cold}}{T_{hot} - T_{cold}} \quad (2)$$

According to convention a positive coefficient denotes a p-type material. While this setup does not account for a contact potential between the probes and semiconductor, it is adequate for measuring relative changes.

Figure 13 shows conductivity and Seebeck coefficient as a function of time at 200°C during the heat/rinse cycles for both Na-free ACIGS and ACIGS with two sequential NaF depositions. The conductivity of the Na-treated sample was two orders of magnitude higher than the Na-free control, while the Seebeck coefficient was an order of magnitude higher than the control. Within 30 minutes of treatment, both measurements decreased to values similar to the Na-free sample. After a second NaF

treatment was carried out, conductivity and Seebeck coefficient returned to their original values before decreasing again with subsequent Na removal, indicating that the effects of Na are reversible. The Na-free sample was subjected to the same heating procedure, and both parameters showed negligible change over the whole experiment, demonstrating that the heat/rinse cycling did not affect the electrical properties of the film. The observation that removing GB Na changed the electrical properties to those very similar to the Na-free sample is strong evidence that Na acts only at GBs to improve device performance with minimal contributions from Na in the grain interior.

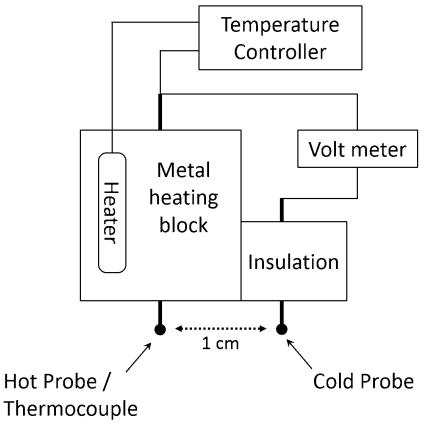

Figure 12. Schematic of the Seebeck coefficient measurement apparatus.

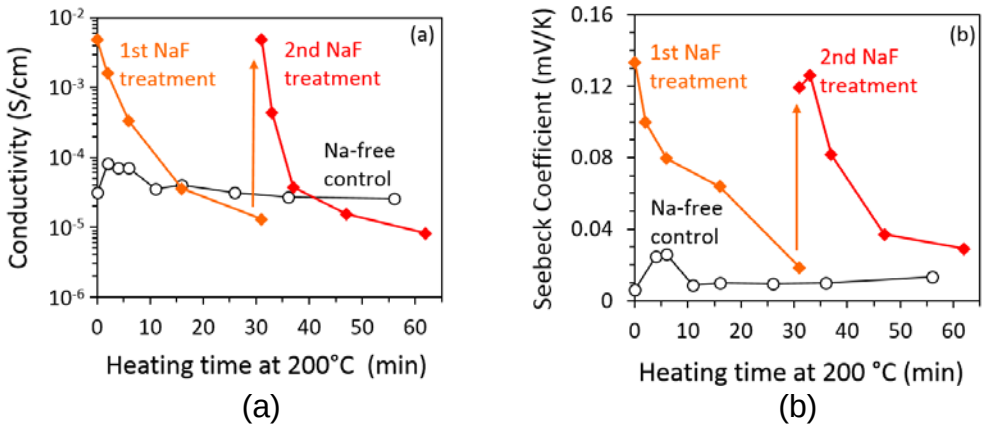

Figure 13. (a) Room temperature ACIGS conductivity and (b) Seebeck coefficient as a function of heating time at 200°C for the Na-free control (open circles), after the 1st NaF treatment (orange diamonds), and after the 2nd NaF treatment (red triangles).

The decrease in conductivity with Na removal is consistent with numerous observations that low Na CIGS films have lower in-plane conductivities [54-56]. The relationship

between conductivity and charge carrier properties can help identify the mechanism for these electronic changes in ACIGS. For a p-type semiconductor, σ can be expressed as

$$\sigma = q(\mu_h p - \mu_e n) \tag{3}$$

where *q* is the elementary charge, *p* and *n* are the concentration of holes and electrons, and μ_h and μ_e are the hole and electron mobility, respectively. In a polycrystalline film this relationship becomes more complex due to the presence of GBs, but the fundamental concepts presented in Eqn. 3 are still valid. Hall mobility measurements from other groups suggest that carrier mobility is not affected by the presence of Na [54], therefore, the decrease in conductivity is due to changes in either electron or hole concentrations. A conductivity measurement alone cannot distinguish between carrier type, concentration, or mobility, therefore additional techniques and measurements are needed to determine which of the carrier properties is sensitive to Na.

The Seebeck coefficient, when measured together with conductivity, can be used to distinguish between these electrical properties. For a p-type semiconductor, the Seebeck coefficient can be expressed as [65]

$$S = \frac{k_B}{\sigma}\left\{-n\mu_e\left[\frac{5}{2} + r_e - \ln\frac{n}{N_c}\right] + p\mu_h\left[\frac{5}{2} + r_h - \ln\frac{p}{N_v}\right]\right\} \tag{4}$$

where k_b is the Boltzmann constant, N_V and N_c are the effective density of states in the valence band and conduction band, respectively, and $r_{e,h}$ is a parameter determined by the carrier scattering mechanism and ranges from -1/2 to 3/2. The Seebeck coefficient remains positive throughout the experiment as expected for a p-type semiconductor. The effect of hole carrier concentration on Seebeck coefficient can be demonstrated more clearly by examining these expressions in the case of a strong p-type material where $p >> n$. In this regime Eqns. 3 and 4 reduce to

$$\sigma = q\mu_h p \tag{5}$$

$$S = \frac{k_B}{q}\left(\frac{5}{2} + r_h - \ln\frac{p}{N_v}\right) \tag{6}$$

From these simplified expressions, conductivity and Seebeck coefficient exhibit opposite trends with respect to hole concentration, as depicted in Figure 14, and a decrease in the acceptor concentration alone cannot explain the observed trends in Figure 13 where both parameters decrease with GB Na removal from ACIGS films. Instead, we propose that Na removal increases compensating electrons, which in turn decreases both conductivity and Seebeck coefficient. This observation that Na suppresses compensating donor defects has also been observed in CIGS thin films [66,67] indicating that the behavior of Na is near identical for both CIGS and ACIGS.

The Na removal procedure was also performed on a series of SLG/Mo/CIGS samples for a total of 6 cumulative hours of heating at 200°C. Although the SLG substrate is a source of Na, diffusion through Mo proceeds too slowly at 200°C to replenish the CIGS. Extrapolating the data discussed earlier, the diffusion length for Na in Mo films after 6

hours of heating at 200°C is 46 nm, much smaller than the 700 nm layer thickness. The SIMS depth profiles presented in Figure 15a show that this procedure lowered the Na concentration by a factor of 4. After the removal procedure, the minimum Na concentration was 3×10^{18} at/cm^3 which is very close to the solubility limit estimated for a Bridgman-grown CIS single crystal (see later discussion) indicating that most remaining Na resides within the grain interiors.

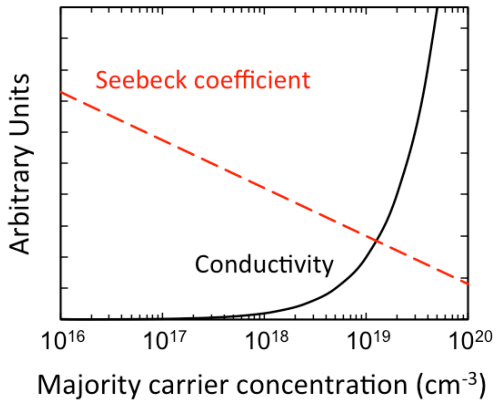

Figure 14: Seebeck coefficient (dashed red line) and conductivity (solid black line) as a function of majority carrier concentration for an arbitrary semiconductor with p>>n from Eqns 5 and 6.

Devices of the structure SLG/Mo/CIGS/CdS/ZnO/ITO/Ni/Al were processed with and without Na removal treatment of the CIGS film. Resultant current-voltage (J-V) plots are shown in Figure 15b, with the device parameters listed in Table 3. Na removal is seen to cause a decrease in V_{OC}, FF, and efficiency to give device performance very similar Na-free devices, confirming the beneficial role of Na in CIGS device performance.

Table 3: J-V characteristics and average Na concentrations of the devices presented in Figure 15.

Sample	Avg. Na Conc. (at/cm^3)	V_{OC} (V)	J_{SC} (mA/cm^2)	FF (%)	η (%)
As-deposited	1.7×10^{19}	0.65	29.8	76.7	14.9
After Na removal	4.1×10^{18}	0.60	28.9	68.6	11.9

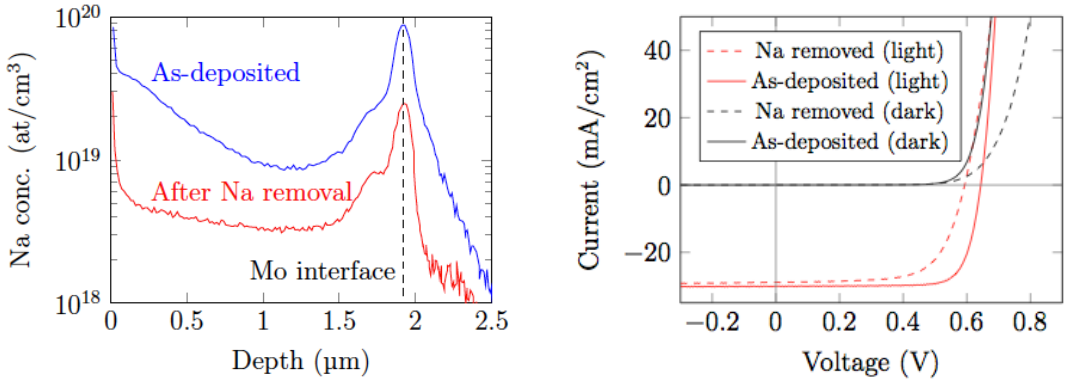

(a) (b)

Figure 15: (a) Na SIMS depth profiles through CIGS for an as-deposited film and after Na removal. (b) J-V curves for CIGS devices with standard Na (solid) and with Na removal (dashed).

In light of these results, any proposed mechanism describing the effects of Na in (A)CIGS must explain the observed reversibility of electrical properties when Na is added and removed. A common explanation for the behavior of Na at GBs is that it reduces compensating donors by catalyzing the formation of O_{Se} [63], acts only as an oxygenation catalyst, and does not directly participate in defect passivation. By this hypothesis the removal of Na alone will have no affect on electrical properties. To reverse the effects of this mechanism, oxygen must also be removed to reform V_{Se} defects. However, O_{Se} is directly bound to In and Ga by very strong and stable In-O and Ga-O bonds. The passivation of V_{Se} with O was calculated to have a standard enthalpy of reaction of −4.3 eV [59], thus it is thermodynamically unfavorable to remove O and reform V_{Se} with Na removal. This mechanism, therefore, cannot explain the observed reversibility of the electrical properties.

Another proposed mechanism that is consistent with the electrical measurements and observed reversibility is that Na replaces donor-type In_{Cu} defects at the GBs to form neutral Na_{Cu}, which results in a net increase in p-type conductivity. The formation of this defect is strongly exothermic, with a free energy in the bulk as low as −1.0 eV, and the reaction proceeds easily [58]. The high solubility of Na compounds in water provides a driving force for the removal of Na_{Cu} during the rinse/heat cycling procedure, which results in the re-formation of the In_{Cu} defects and causing a conductivity decrease. Additional work is needed to conclusively determine the defects responsible for the observed behavior.

Donor defects at GBs can be detrimental to device performance [60,61]. Donor defects are positively charged after losing their electrons, which causes downward band bending along the grain surfaces of p-type (A)CIGS (Figure 16a). Downward band bending creates depletion regions extending from GBs, which can significantly lower the hole concentration in small grains [61]. Electrostatic repulsion from positively charged

GBs creates an energy barrier for holes moving between adjacent grains and this energy barrier contributes to the lower conductivity observed in the Na-free samples. Additionally, photogenerated electrons are attracted to positively charged GBs where they can recombine, resulting in lower V_{OC} and FF. Device simulations that account for electron attraction to positively charged GBs show significant improvements in device performance with the passivation of GB defects [60]. Na passivates donor defects, creating flat bands along GBs and eliminating the detrimental positive charge. Downward band bending near GBs has been confirmed using KPFM [68]. The potential barrier in Na-free films could be as high as 300 meV, while films with Na typically had barriers below 100 meV [56,69,70], further supporting Na passivation of donor-like defects at GBs.

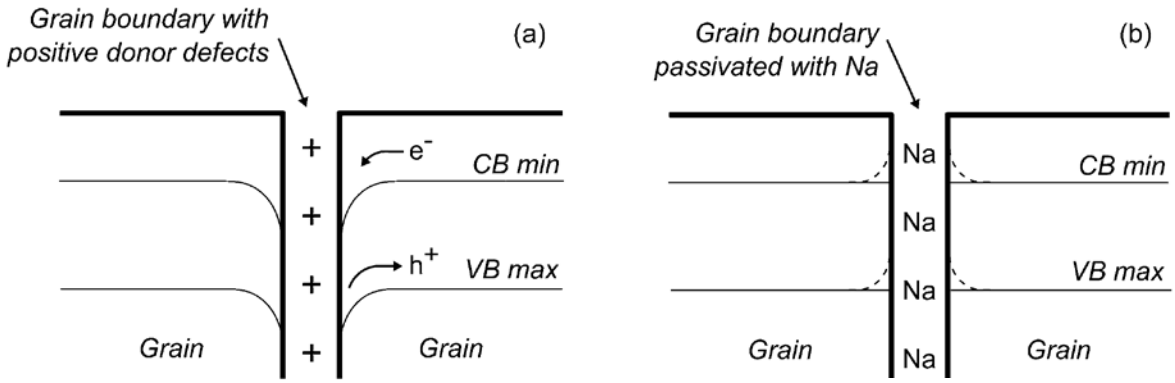

Figure 16: Band diagram of the GB region in CIGS. A positively charged grain boundary (a) repels holes creating a depletion region and attracts electrons increasing recombination. Na can passivate donor defects at GBs (b) eliminating the depletion region, possibly creating accumulation regions (dotted lines), and decreasing electron recombination.

The amount of positive charge can be roughly estimated from the density of donor defects at the GBs as shown in Eqn. 7, assuming a uniform donor density and that each donor provides two electrons. While there are more rigorous treatments for estimating GB charge, this approach provides a suitable first approximation.

$$Q_{GB} = 2qN_D^{GB} \tag{7}$$

where Q_{GB} is the GB surface charge density, q is the elementary charge, and N_D^{GB} is the surface density of donors along GBs. From Q_{GB}, the space charge width (w_{sc}) can be estimated by maintaining charge neutrality between the GB and the space charge region

$$Q_{GB} = N_A q w_{sc} \tag{8}$$

The magnitude of the band bending induced by the space charge region (V_b) can be estimated by solving Poisson's equation for a uniform doping density, N_A, and evaluating the solution at the GB giving

$$V_b = \frac{qN_A}{2\epsilon} w_{sc}^2 \quad (9)$$

where ϵ *is* the absolute dielectric constant for CIGS. From Eqns. 7-9, the 300 meV barrier height observed in a Na-free GB gives a space charge width of ~100 nm and a GB donor density of ~5x10^{11} cm^{-2}, assuming N_A = 10^{17} cm^{-3} and the relative dielectric constant is 7.5 [70]. The dangling bond density of a typical CIGS surface is ~10^{15} cm^{-2}, so under the stated conditions only a small fraction of surface sites need to be electrically active. In the case of a Na-containing GB with a barrier height of 100 meV, the GB donor density is calculated to be ~3x10^{11}. Therefore, to reduce the barrier height below 100 meV, ~40% of active donor sites need to be passivated with Na. While the exact numbers may vary from film to film, this example demonstrates the feasibility of forming a depletion region from GB donor states.

The work related to understanding the mechanisms of Na in CIGS GBs was published during the project [66,71,87].

B. Task 2.0: Na Incorporation in Single Crystal CIGS

1. Diffusion in CIS single crystals:

While it is well established that Na in CIGS resides primarily at GBs, it has not been conclusively ruled out that very small amounts of Na within grain interiors affect device performance. Niles et al. [32] showed with high resolution AES that Na is only detectable at GBs and measurements made on grain interiors fall below detection limits. However, the detection limit in this study was only ~0.1 at% and concentrations below this could still significantly affect changes in the electronic properties. For example, it has been shown that addition of Na in CIGS can increase net carrier concentration from 2.4 × 10^{14} cm^{-3} to 6.5 × 10^{15} cm^{-3} with an 85 mV V_{oc} increase [6]. An increase of this magnitude could easily be achieved by incorporation of Na in the bulk grains at concentrations that are well below the 0.1 at% detection limit.

Recently very small amounts of Na were detected within grain interiors using APT, a technique that creates a three-dimensional elemental map with sub-nanometer spatial resolution and a detection sensitivity of a few tens of atomic ppm [72]. Its low detection limits and fine spatial resolution make APT an ideal technique for distinguishing between Na in GBs and grain interiors. ATP measurements on polycrystalline CIGS confirm that a majority of Na resides along GBs, but small amounts of Na are also present in the interiors at concentrations ranging from 30 ppm to 145 ppm [33,73-75]. Despite confirming the presence of in-grain Na, current APT methods are not well suited

to characterizing lattice diffusion of Na within the grain interior. This is partly due to the small size of APT samples, which typically consist of a cone that is 500 nm across and 100 nm at the base. These small samples are usually not representative of the entire film, and coupled with the difficulty of sample preparation, make a comprehensive diffusion study with this technique impractical. Despite this, these measurements do provide insight into the behavior of Na in the CIGS grain interior. APT usually shows a uniform Na concentration in the grain interior throughout an entire sample, suggesting that lattice diffusion occurs fast enough that the grain is Na-saturated. Another study detected Na in grain interiors after a NaF post deposition treatment at 157°C, suggesting that Na lattice diffusion is rapid even at low temperatures [76].

Single crystals are ideal for studying bulk lattice diffusion since a larger analysis area can be used, without interference from GBs, allowing depth-profiling techniques, e.g. SIMS, to be used to analyze diffusion. Schroeder and Rockett [67] incorporated Na into epitaxial single crystal CIGS from both Na_2Se and NaOH at temperatures up to 600 °C and reported Na concentrations ranging from 6×10^{19} cm^{-3} to 10^{20} cm^{-3}, though characterizing diffusion was not the objective of the study.

In this project, the diffusion of Na into CIS single crystals was investigated by evaporating NaF directly onto the surfaces followed by heating to drive Na into the sample. Diffusion was evaluated at two different temperatures and a lattice diffusion E_a was estimated. The diffusion mechanism is investigated by comparing the diffusion behavior of Na in two crystals with different defect structures.

Single crystals of CIS grown by both vertical Bridgman and horizontal gradient freezing, or melt grown, methods were used to evaluate the incorporation of Na. Table 4 presents the atomic composition of each crystal by x-ray fluorescence spectroscopy (XRF), and shows the melt-grown crystal is stoichiometric and the Bridgman-grown crystal is slightly Cu-poor. The standard deviation for the measurement is ~0.1at%, therefore, the difference in Cu content is statistically significant. CIS made by the vertical Bridgman method is typically Cu-poor due to the segregation of Cu_2Se during growth.

Laue crystallography images for each crystal are shown in Figure 17 and both show clearly defined diffraction spots confirming that both samples are single crystals. Each image also shows mirror symmetry, due to a terminating mixed cation-anion face. SEM images showed no indication of GBs or micro-cracks (not shown).

Table 4: Composition for the CIS single crystals.

Crystal	Cu [at%]	In [at%]	Se [at%]	Cu/In	Metals/Se
Bridgman	24.2	26.1	51.3	0.93	0.98
Melt	25.1	25.5	49.9	0.98	1.01

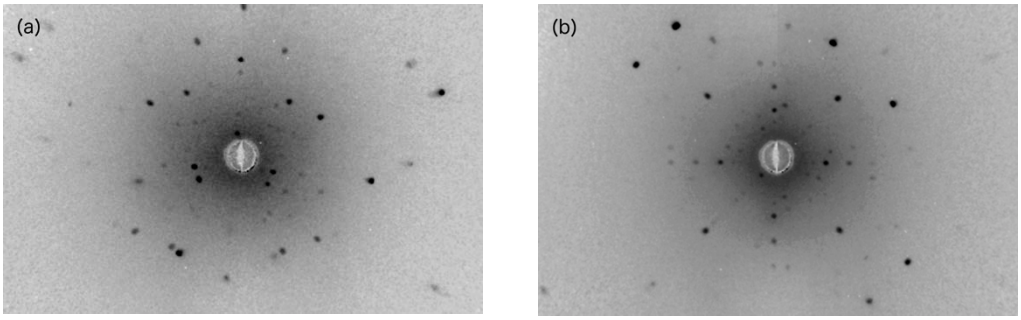

Figure 17. Laue crystallography images of (a) Bridgman grown and (b) melt grown CIS single crystals.

The crystals were mechanically polished prior to diffusion treatment. ~40 nm of NaF was then deposited on the crystals by evaporation through a 4 x 4 mm^2 mask. After NaF deposition, the crystals were heated at 420 °C for 300 min, without breaking vacuum, to induce diffusion. After this treatment, excess NaF was rinsed from the surface with DI water and the concentration profile measured with SIMS. The crystals were recycled by repeating the polishing, deposition and diffusion procedure on the backside of each crystal with a 480 °C heat treatment. The mechanical polishing eliminated any possible Na contamination from the first experiment.

Figure 18 shows Na concentration profiles for both crystals after the diffusion treatments. The Na concentration profile on the uncoated area of the Bridgman crystal after heating at 420 °C (Figure 18a) is two orders of magnitude smaller than in the NaF-coated area of the same crystal. The residual amount of Na observed on the uncoated area is likely due to contamination either during crystal growth or during NaF deposition. The depth profile was modeled using the solution for diffusion from a constant source into a semi-infinite, and the best-fit line depicted in these figures was obtained by varying the lattice diffusion coefficient (D_g) and source concentration (c_0) from the solution

$$c(z,t) = c_0 \mathrm{erfc}\left(D_g t\right) \qquad (10)$$

where *z* is depth and *t* is diffusion time. Na has a limited solubility in CIS and c_0 represents the solubility limit. The semi-infinite slab model is justified because the crystal is much thicker than the diffusion length and 40 nm of NaF provides much more Na than what ultimately diffuses into the crystal.

Within the first few micrometers of each profile, the concentration steeply decreases in a manner that does not follow Eqn. 10. This is likely caused by an increase in defects near the surface that were introduced by the mechanical polish. For this reason z = 0 was set further into the crystal rather than at the surface. The optimized values for D and c_0 are shown in Table 5.

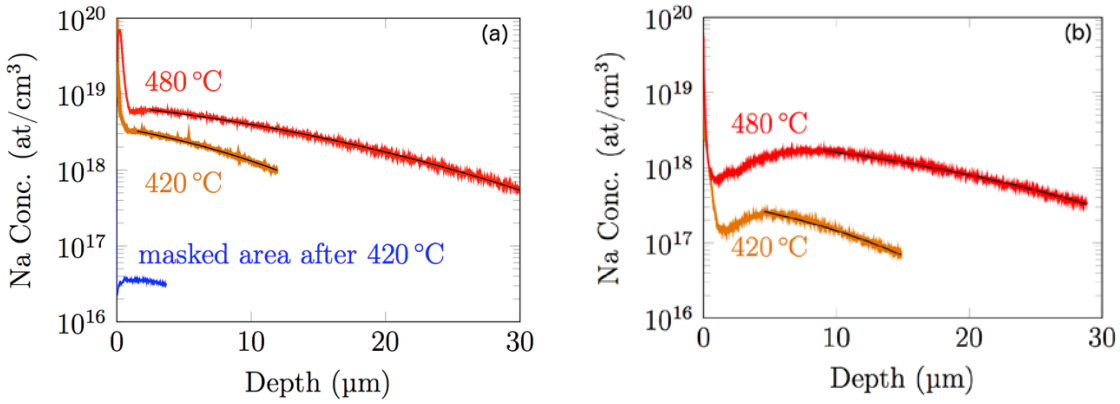

Figure 18. SIMS Na depth profiles on the NaF-coated areas of the (a) Bridgman grown CIS and (b) melt grown CIS after heating at 420°C (orange) and 480°C (red) along with best fit lines (black). The Na profile on the uncoated area of the Bridgman crystal is shown in blue.

Table 5. D_g and c_0 of Na in CIS single crystals obtained from the best fits of Eqn. 10 to the Figure 18 depth profiles.

Crystal	Temperature [°C]	D_g [cm^2/s]	c_0 [cm^{-3}]
Bridgman	420	2.4×10^{-11}	3.3×10^{18}
Bridgman	480	6.0×10^{-11}	6.2×10^{18}
Melt	420	2.0×10^{-11}	2.7×10^{17}
Melt	480	5.4×10^{-11}	1.7×10^{18}

D_g is nearly identical for both samples and is comparable to the those measured in other studies for both Na and Cu in CIS. One study estimates both D_b and D_g of Na in polycrystalline CIGS using SIMS [76] where the D_g at 400°C was 9×10^{-12} cm^2/s, comparable to that measured at 420°C in this work. Another study directly measures a D_g of 10^{-10} cm^2/s for Cu diffusion in single crystal CIS at 400°C using a radioactive tracer technique [77]. Na^+ is ~25% larger than Cu^+ and, therefore, it is not surprising that Na diffusion is slower.

As diffusion was only measured at two temperatures, these experiments cannot determine if Na diffusion in CIS has an Arrhenius relationship. The E_a for diffusion of Na in single crystal CIS is estimated to be 0.69 eV for the Bridgman crystal and 0.74 eV for the melt-grown crystal. As E_a was only estimated from two temperatures, which introduces a large margin of error, so these values are not statistically different. The

solubility of Na in the melt-grown crystal was shown to be almost 10x lower with a stronger temperature dependence compared to the Bridgman crystal.

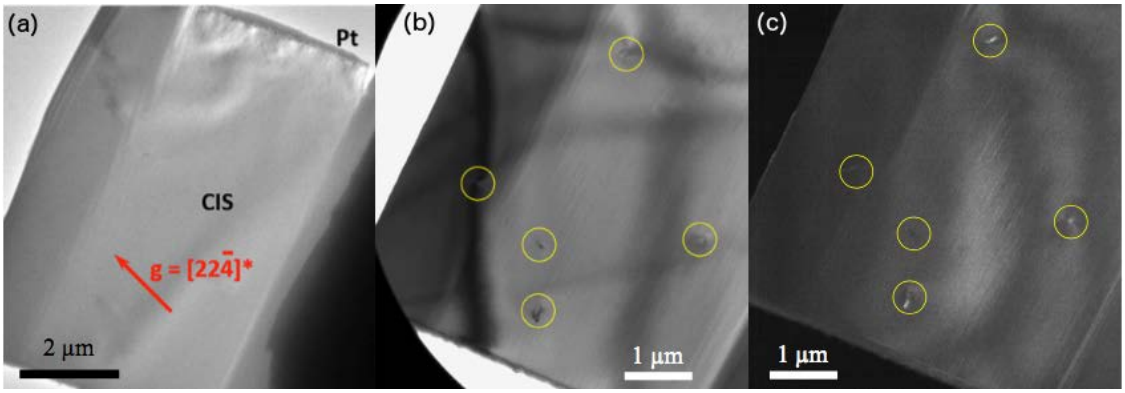

Figure 19: A series of BF and DF TEM images of the Bridgman crystal taken under two-beam condition. (a) A multi-beam BF image with no apparent contrast of dislocations. (b) and (c) are a pair of BF and DF images from the same region with dislocations circled.

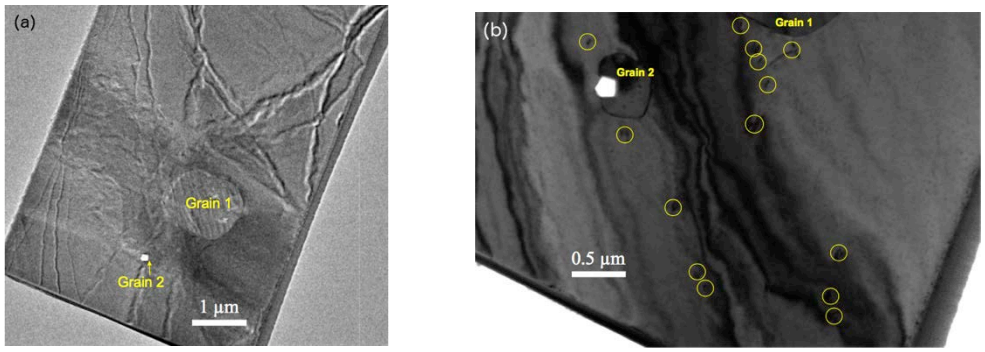

Figure 20: A series of BF and DF TEM images of the melt grown crystal taken under two-beam condition. (a) A multi-beam BF image showing two isolated grains embedded in the CIS matrix, and (b) a BF image with dislocations circled.

Extended defects, which strongly affect diffusion behavior, were evaluated using transmission electron microscopy (TEM) by the U. of Illionois group, to measure the dislocation density of each crystal. TEM samples were prepared by a lift-out method in a focused ion beam instrument. TEM bright field (BF) and dark field (DF) images were taken under a two-beam condition with the deviation parameter, s, slightly positive. The dislocations in the crystals can be distinguished by comparison of two beam DF images and the corresponding BF images shown in Figures 19 and 20 for the Bridgman and melt grown samples, respectively. A higher dislocation density was observed within 1 µm of the surface (not shown), which is likely caused by the mechanical polishing.

The melt grown specimen clearly has a much higher dislocation density and also has two isolated grains embedded in the CIGS matrix. The striation pattern in the larger grain is likely caused by a high density of stacking faults. The estimated dislocation densities from these TEM images are 10^7 cm^{-2} and 10^8 cm^{-2} for the Bridgman and melt grown crystals, respectively. Extended defects are expected to increase diffusion and solubility. However, the melt grown crystal has a lower Na solubility with the same diffusion coefficient (Table 5), despite having a higher dislocation density. This suggests that dislocations are not controlling Na diffusion in the CIS crystals.

Diffusion through dislocations can be classified using the same system originally proposed by Harrison for GB diffusion [78,79]. Diffusion by this mechanism is classified by three regimes, types A, B, and C, based on the relationship between the bulk lattice diffusion distance ($D_g t$), the mean distance between locations (Λ), and the dislocation core width (a). Type A occurs when $D_g t > \Lambda$ and diffusion appears to follow Fick's laws with D_g a volume-weighted combination of the bulk and dislocation diffusion. Type B occurs when $\Lambda >> D_g t$ and diffusion can be modeled using an isolated dislocation model. Depth profiles in this regime exhibit a tail where the natural log of concentration is linear with depth. Type C occurs when $\Lambda >> D_g t$ and diffusion is constrained to the dislocations, following Fick's laws, with minimal diffusion into the bulk. Concentrations are typically smaller than type A and B due to the small volume fraction of dislocations.

Considering the results for the CIS samples, the dislocation density in both crystals is too low to accommodate the amount of measured Na, therefore, diffusion cannot proceed by the type C regime. If dislocation cores are approximated as cylinders with a diameter of 1 nm, the volume fraction occupied by dislocations with a density of 10^8 cm^{-2} would be ~8×10^{-7}. If dislocation cores were entirely occupied with Na, this volume fraction would correspond to a concentration ranging from ~10^{16} cm^{-3} to 10^{17} cm^{-3}, considerably lower than measured concentrations for either crystal. EDS measurements taken at dislocations did not detect Na, confirming that no significant accumulation occurs at these areas.

The depth profiles (Figure 18) indicate that type B diffusion is also unlikely. The dislocation tail for type B diffusion becomes prevalent at depths greater than ~3x the diffusion length. The average distance between dislocations can be approximated as the inverse of the square root of the dislocation density, assuming that dislocations are randomly located. This approximation gives an average dislocation distance of 3 μm for the Bridgman crystal and 1 μm for the melt grown crystal. If type B diffusion is occurring, the bulk diffusion length must be less than this and a dislocation tail should become prevalent at a depth greater than 9 μm for the Bridgman crystal and 1 μm for the melt grown crystal. The logarithm of the concentration profile beyond either of these distances is clearly not linear in either crystal confirming that diffusion is not type B.

As the depth profiles are not consistent with types B and C, Na diffusion in these CIS single crystals must follow type A kinetics. The apparent D_g measured for type A transport is an average between the dislocation and bulk diffusion coefficients weighted by their respective volume fractions. With a dislocation volume fraction of 10^{-7}, the contribution of diffusion along dislocations is negligible.

A possible mechanism for Na diffusion in CIS is a vacancy-substitution pathway where Na moves through the CIS bulk by a series of exchanges with vacancy sites. This mechanism would likely be mediated through Na on a Cu vacancy (Na_{Cu}) as Cu and Na are monovalent. DFT calculations show that the substitution of Na with Cu is more favorable by ~1 eV to 2 eV compared to substitution with In or Se [80]. If diffusion is mediated entirely with Cu vacancies (V_{Cu}), an increase in their concentration would cause an increase in D_g. The Bridgman crystal has a lower Cu content and should show a corresponding V_{Cu} increase. However, both crystals show nearly identical D_g. This suggests that V_{Cu} does not control the diffusion of Na in CIS. Furthermore, the unusually low E_a is inconsistent with a vacancy-mediated mechanism. The measured E_a for a vacancy-mediated diffusion mechanism will be a combination of energies for vacancy formation, vacancy migration, and solute site exchange. The migration barrier for V_{Cu} in CIS has been calculated to range from 1.09 eV to 1.26 eV [81,82], inconsistent with the E_a estimated in this study. Another possible mechanism is interstitial diffusion, which typically has E_a lower than vacancy-mediated substitutional mechanisms. For example, E_a for migration of Cu interstitials in CIS is only 0.2 eV to 0.34 eV [81-83]. However, the large size of Na^+ ions (1.16 Å) compared to other host ions (Cu^+:0.91 Å, In^{+3}:0.94 Å, Se^{-2}:1.84 Å) will cause a low equilibrium concentration of Na interstitials, inconsistent with the measured solubility.

This disagreement between a low E_a and high solubility can be explained using a hybrid interstitial-substitutional diffusion mechanism. In a hybrid mechanism most solute atoms reside on host lattice vacancies and only a small fraction of solute atoms exist interstitially [79] as shown in Figure 21. The interstitial diffusion is much faster than vacancy-substitutional diffusion, allowing for a relatively high solubility along with fast bulk diffusion. This mechanism was first experimentally confirmed for Cu diffusion in Ge [84] and it has been speculated that Cd and Fe diffusion in CIGS grains both proceed by an interstitial-substitutional mechanism [85,86]. These diffusion studies involved solute atoms that were similar or larger in size than the host solvent atoms.

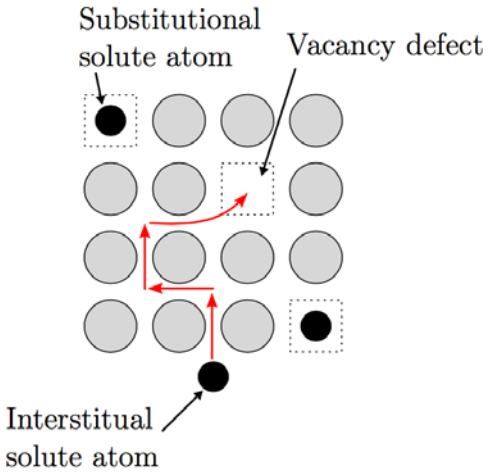

Figure 21: Illustration of a hybrid interstitial-substitutional diffusion mechanism for an arbitrary solute/solvent system.

As the rate of Na diffusion is controlled by interstitial transport, both crystals have comparable D_g despite having different Cu contents. The higher V_{Cu} concentration in the Cu-poor Bridgman crystal allows it to accommodate more Na as observed by the increased solubility limit. The melt grown crystal exhibited a stronger temperature dependence because Cu-rich CIS has a greater V_{Cu} formation enthalpy, 1.43 eV, compared to Cu-poor CIS, 0.64 ± 0.15 eV [81]. E_a for Na solubility estimated from SIMS is 1.4 eV for the melt-grown crystal and 0.48 eV for the Cu-poor Bridgman crystal, both in good agreement with V_{Cu} formation energies for Cu-rich and Cu-poor CIS, respectively. Measurements at additional temperatures are needed to confirm that Na solubility has an Arrhenius relationship with temperature.

The results from this study are in good agreement with literature DFT calculations. Oikkonen et al. [81] calculate an E_a for interstitial Na diffusion of 0.51eV, which is within experimental error of the 0.7 eV value estimated in this study. Oikkonen notes that Na_{Cu} has a more favorable formation enthalpy compared to interstitial Na and proposes a hybrid interstitial-substitutional mechanism that is consistent with this study.

Na diffusion into single crystals provides insight into Na diffusion in polycrystalline grain interiors. The estimated diffusion coefficients demonstrate that Na will be easily incorporated into the grain interiors of polycrystalline CIGS even at lower temperatures. NaF post-deposition treatments typically involve heating NaF-coated CIGS for 30 min at temperatures ranging from 300 °C to 400 °C. Using the information in Table 5, the diffusion length after 30 min of heating extrapolated at 300°C is 0.6 μm, with Na penetrating significantly into the grains. When Na is incorporated during growth, such as from the substrate or Na-precursor, at growth temperatures as high as ~600°C for times up to 1 h, a diffusion length of ~9 μm is determined. This is significantly greater than the largest grains in CIGS films, indicating that grains will be uniformly Na-saturated when manufactured under standard processing conditions.

We recently provided evidence that the effects of Na on CIGS electrical properties are due to its presence at the GBs rather than the interiors [87]. This suggests that Na in grain interiors either does not significantly affect electrical properties or has a negative effect. There is evidence that too much Na in CIGS can have a detrimental effect on device performance. This could be a result of Na annihilating V_{Cu} in the bulk and reducing the net carrier concentration. The lower temperature used for PDT prevents significant Na incorporation into the bulk, so these detrimental effects are not observed. When SLG is the Na source, the lower Na levels prevent high concentrations in the grains. More experimental evidence is needed to confirm that Na can detrimentally impact CIGS in this way.

The work on Na diffusion in CIS single crystals was submitted for publication during the project [88].

2. Na and K diffusion into epitaxial CIS layers

There have been recent notable efforts to improve the performance of CIGS cells with the incorporation of K into the absorber layers [89,90]. Results have been promising, but the role of K in device performance improvements and possible synergistic effects when co-doping with Na are poorly understood. To begin to understand these effects, experiments were conducted at U of Illinois on diffusion of Na and K into epitaxial CIS single crystals to analyze their effects on cathodoluminescence (CL) of the resulting films. As part of these experiments, measures of Na and K diffusivity in CIS were also obtained.

Epitaxial single crystals of CIS were grown on GaAs (100)-oriented substrates using a hybrid sputtering and evaporation method under typical process conditions. Films of 1.3 µm thickness were grown with composition of 22% Cu, 26% In, and 52% Se, with small quantities of Ga detected from out-diffusion from the substrate. A typical SEM image of an epitaxial layer surface is shown in Figure 22. The surface is very smooth compared to polycrystals, but exhibits striations along one of the (110) type directions in the surface plane.

The grown films were cut into individual pieces for further analysis. One sample was held as an untreated control, while others were annealed in dry N_2 in a tube furnace in the presence of either NaF or KF for between 10 min and 1 hour at 400, 500, and 600°C. Heating ramp-up took between 7 and 15 min depending on treatment temperature. Samples were cooled to below 200°C within 15 minutes. For comparison some samples were also annealed on a graphite boat in the furnace without intentional Na or K addition.

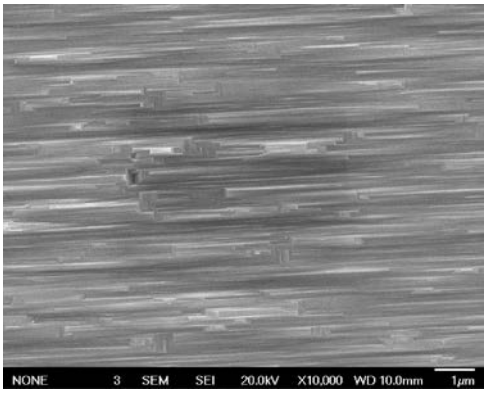

Figure 22: SEM image of an epitaxial CIS layer surface showing it to be very smooth with faceted ripples along one of the (110) directions. Scale bar indicates 1 µm.

Analysis of the treated films showed typical diffusion profiles (not shown), following a complementary error-function shape for Na after 10 min anneals at each temperature.

The diffusivity was determined to range from $4x10^{-10}$ cm^2/s at 400°C to $3x10^{-9}$ cm^2/s at 600°C by fitting the resulting profiles. These values were between 2 - 10 times greater than previously reported, with the difference being greater at the higher temperatures. The E_a for Na diffusion in CIS was calculated to be 0.49 eV, very similar to results for Na diffusion in CIS single crystals at IEC (discussed above). The diffusivity for K was found to range from $5x10^{-10}$ to $7x10^{-9}$ cm^2/s. However, a clear trend from which E_a could be extracted was not obtained.

As-deposited and annealed samples were measured by spectroscopic CL at 5 K, with 20 keV beam energy and beam current ranging from 0.1 to 100 nA. The emissions (Figure 23) consist of a number of identifiable components. The sub-bandgap emissions appear to have components at near constant energies for all measurement conditions, though with a change in relative intensity as beam current is increased. The lowest energy contribution to the emissions was at ~840 meV. This has been seen previously and is suggested to correspond to a donor-acceptor-pair transition between a shallow donor and the primary acceptor in the material. A significant emission also occurs at ~880 meV. Both of these emissions do not change significantly as a fraction of the total emission spectrum when the samples were annealed with NaF or KF. At higher beam currents these peaks contributed to a decreasing fraction of the total emission intensity. A peak at 930 meV was observed that has previously been connected to a free-to-bound transition between the shallow donor and the valence band edge. This peak increased significantly in intensity for the lowest beam current for all anneal treatments, with the greatest increase observed for the NaF anneal. At higher beam currents this peak remained a near constant weak contribution to the total emission. Emissions at 970 and 1020 meV were also observed, likely due to free-to-bound and band edge-to-band edge emissions, respectively. Higher energy emission tails were observed for all spectra with the tail of the highest energy emissions decreasing near exponentially with increasing energy.

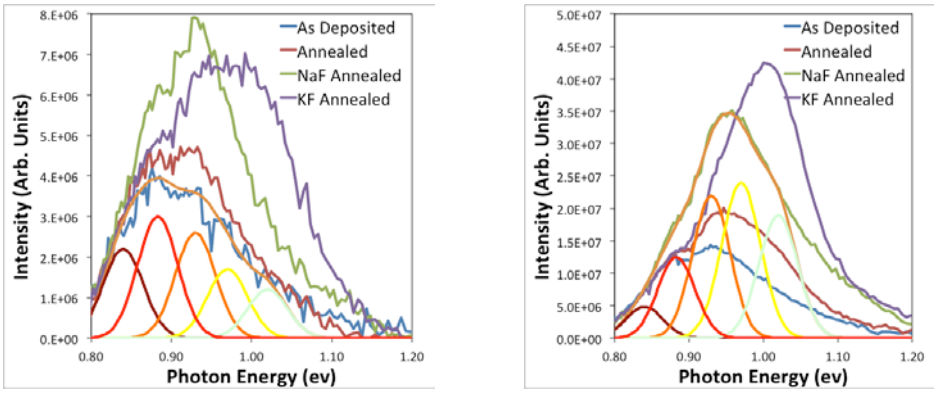

Figure. 23. CL spectra showing the effect of annealing CIS epilayers with and without NaF or KF at 600°C for one hour. (a) The spectra obtained at 100 pA beam current and (b) the spectra obtained at 1 nA. No peaks were fit above ~1eV as this is above the energy gap of the material and all spectra showed a roughly exponential tail in emissions above the energy gap emission.

In all cases the samples annealed with KF showed the highest intensity emission at the highest emission energy and with significant increases in intensity, in particular, for emissions associated with bands or band tails. Samples annealed with NaF showed similar increases in emission in the higher energy components but with greater intensity in the donor-acceptor pair transitions or free-to-bound transitions than in the band-to-band transitions.

The emission spectra shift to higher energy approximately logarithmically with increasing beam current, as would be expected if the beam is filling states and the quasi-Fermi energy of minority carriers is increasing through the band edge. This is consistent with the observation of increasing amounts of above-band-gap emission intensity as the beam current increases. The peak energy is higher for the samples annealed with KF, followed by samples annealed with NaF, than those annealed without intentional addition of Na or K, and the as-grown samples have the lowest peak energies. The integrated emission intensity overall increases approximately quadratically with increasing beam current, indicating a decreased emission efficiency. The quadratic dependence suggests that non-radiative recombination is increasing as the square of the carrier density.

Based on these results we conclude that annealing the samples with NaF and KF increases the emission intensity significantly for all conditions tested to date, and that the increase primarily involves transitions to or from band-edges. We propose that the cause of the change is the sharpening of the energy band edges. Because the donor-acceptor-pair transitions do not seem to change significantly, we do not anticipate that alkali metals strongly influence the associated point defects, although the overall increase in luminescence presumably resulted from a reduction in non-radiative recombination pathways, though the mechanism is not identified at this time. The results are consistent with observations that photovoltaic device performances improve with reduced band tail width and density of states.

C. Task 3. Effect of Na in Devices Fabricated on CIGS Processed by Precursor Selenization.

The objective under this task was to determine the effects of Na in CIGS films process by reaction of sputtered precursor metal films in H_2Se/H_2S gases. The nature of the absorber processing would allow film conversion to be interrupted in order to monitor the CIGS growth sequence. Unfortunately, the start of this task was delayed due to a major upgrade of the selenization reactor. Preliminary results did confirm similar effects due to Na were observed in selenized precursor films as for co-evaporated CIGS. However, progress was hindered due to several groups and projects using the seleniztion system. We found the co-evaporated and single crystal work to be a very rich source of research and efforts on Task 3 were abandoned.

CONCLUSIONS:

Task 1.0: Effect of Na in Devices Fabricated on PVD Deposited CIGS.

Na Diffusion Through the Mo Back Contact Layer: By selectively adding or removing oxygen from the surface of Mo-coated SLG, a linear relationship was determined between surface oxygen and Na accumulation levels. Na diffusion was modeled to determine D_b. An apparent E_a was calculated to be 117 kJ/mol, which is very similar to that for breaking Mo-O bonds in MoO_3, suggesting these bonds are involved in Na diffusion in Mo GBs. This result, along with the observed increase in Na saturation concentration for films with large surface oxygen levels, shows that oxygen provides the chemical driving force for the Na diffusion through Mo, and suggests Mo substrates could undergo oxidative treatments prior to CIGS deposition to optimize Na incorporation.

Reversibility of ACIGS electrical properties: The effects of Na on the electrical transport properties of ACIGS thin films were investigated using a novel back contact pattern that allows both conductivity and Seebeck coefficient measurements on a single sample. Na was incorporated by NaF evaporation, then removed by several heat/rinse cycles, resulting in a decrease in both measurements until comparable with Na-free ACIGS. This observation is consistent with an increase in compensating donor defects. As the rate of diffusion is low at the temperatures used, the changes in electrical properties are due to the removal of Na from GBs rather than the grain interiors. The Na effects on the electrical properties were shown to fully reversible with the subsequent addition and removal of Na and, therefore, cannot be attributed to the oxygen passivation of V_{Se} due to the stability of resultant In-O and Ga-O bonds. Instead, Na must passivate other donor-like defects, for example replacing In_{Cu} with neutral Na_{Cu}, at CIGS GBs. These complexes can be removed with water rinsing to produce the observed reversibility.

All milestones were accomplished under Task 1 and were reported in previous RPPR1 documents

Task 2.0: Na Incorporation in Single Crystal CIGS

Diffusion in CIS single crystals: Bridgman and melt grown CIS single crystals were used as model systems to represent the grain interiors of a polycrystalline CIGS film. Diffusion was studied by evaporating NaF on the crystal surfaces, followed by heating to 420 °C and 480 °C, and monitoring the Na concentration profiles into the grains. The Na concentration of the treated areas was two orders of magnitude greater than the uncoated control area, demonstrating that the NaF treatment successfully incorporated Na into the crystals. E_a of diffusion was ~0.7 eV for both crystals, while the Na solubility varied by an order of magnitude between the two samples. This is explained in terms of a hybrid interstitial-substitutional diffusion mechanism for Na into CIS. The rate of diffusion is controlled by the diffusion of interstitial Na, explaining why both crystals exhibit the same E_a of diffusion, which is similar to literature values for interstitial Na diffusion in CIS. Importantly, these results indicate that the grains of polycrystalline CIGS films will be Na-saturated when manufactured under standard conditions.

Milestones under Task 2, subtask 2.1 were accomplished and previously reported. The Go/No Go criteria fell under this subtask and this was satisfied with i) the demonstration of Na incorporation in single phase epitaxial CIS films at compositions used for photovoltaic quality thin films at the University of Illinois, and ii) determination of the experimental picture of how Na influences CIGS device performance when supplied by the substrate or from co-evaporated NaF. These accomplishments were presented in past RPPR1 reports and in the continuation report.

Milestones under subtasks 2.2 were not completed. Under subtask 2.3 were achieved with the processing of Na-doped U. of Illinois epitaxial CIS into devices at IEC and was reported.

Na and K diffusion into epitaxial CIS layers CL measurements of CIS films with incorporated Na or K showed an increase in emission intensity involving transitions to or from band-edges. The overall increase in luminescence presumably resulted from a reduction in non-radiative recombination pathways, though the mechanism is not clear, which is consistent with observations that photovoltaic device performances improve with reduced band tail width and density of states.

Task 3. Effect of Na in Devices Fabricated on CIGS Processed by Precursor Selenization.

Milestones under subtask 3.1 were completed and reported. Milestones under subtask 3.2 were not accomplished as described above in the Project Description.

BUDGET AND SCHEDULE:
This project was completed by the University of Delaware over the time period from 09/01/2011 to 8/31/2015. The total project budget was $ 960,000 with no cost share. There were total expenditures of $ 960,000. The original end date was 11/30/2014 and a no cost extension was granted making the end date 08/31/2015.

PATHWAY FORWARD:
At this time, this project has completely wrapped up at both IEC and U. of Illinois. There are currently no plans in place to continue research specifically on the fundamental science of the effects of Na in CIGS solar cells. As Na treatments are necessary for manufacturing high performance devices, optimization of Na treatments will remain an important aspect of any future (A)CIGS-related projects. No patents were prepared under this opportunity. Currently there are no technology transfer or commercialization plans or opportunities directly related to this project.

Despite the success of this project there are still a number remaining questions related to further the understanding and optimization of the chemistry of Na in these devices and materials. These include further elucidating the mechanisms of Na passivation in CIGS GBs, including identifying which defects are involved, and determining if the

presence of Na, its possible chemistries, and effects on device performance and quality at the CIGS/CdS junction and/or in the front transparent contacts.

REFERENCES:

[1] R. Caballero, C. Kaufmann, T. Eisenbarth, T. Unold, S. Schorr, R. Hesse. R. Klenk, and H.W. Schock, Physica Status Solidi A, 206 (2009) 1049–1053.
[2] J. Hedström, O. Håkan, B. Marika, A. Kylner, L. Stolt, D. Hariskos, M. Ruckh, and H.W. Schock, in *Proceedings of the 23rd Photovoltaic Specialists Conference*, p. 364–371, Piscataway, 1993. IEEE.
[3] R.J. Matson, J.E. Granata, S.E. Asher, and M.R. Young, *AIP Conference Proceedings*, 542 (1999) 542–552.
[4] M. Igalson, A. Kubiaczyk, P. Zabierowski, M. Bodegård, and K. Granath, *Thin Solid Films*, 387 (2001) 225–227.
[5] M. Bodegård, K. Granath, and L. Stolt, *Thin Solid Films*, 361-362 (2000) 9–16.
[6] D. Rudmann, A.F. da Cunha, M. Kaelin, F. Kurdesau, H. Zogg, A.N. Tiwari and G. Bilger, *Appl. Phys. Lett.*, 84 (2004) 1129 – 1131.
[7] V. Probst, J. Rimmasch, H. Harms, W. Riedl, J. Holz, and F. Karg, in *13th European Photovoltaic Solar Energy Conference*, p. 2123–2126, Nice, Oct. 1995.
[8] M. Bodegärd, J. Hedström, K. Granath, A. Rockett, and L. Stolt, in *13th European Photovoltaic Solar Energy Conference*, p. 3–6, Nice, Oct. 1995.
[9] T. Nakada, D. Iga, and H. Ohbo. *Jpn. J. Appl, Phys*., 36 (1997) 732-737.
[10] J.E. Granata and J.R. Sites in *Proceedings of the 2nd World Conference on Photovoltaic Solar Energy Conversion*, p. 604–607, Vienna, 1998.
[11[R. Kimura, T. Mouri, and T. Nakada. *Jpn. J. Appl. Phys*., 38 (199) 289–291.
[12] D. Braunger, D. Hariskos, G. Bilger, U. Rau, and H.W. Schock, *Thin Solid Films*, 362 (2000) 161–166.
[13] D. Rudmann, G. Bilger, M. Kaelin, F.J. Haug, H. Zogg and A.N. Tiwari, *Thin Solid Films*, 431-432 (2003) 37–40.
[14] U. Rau, M. Schmitt, F. Engelhardt, O. Seifert and J. Parisi, in *25th IEEE Photovoltaic Specialist Conference*, p. 1005–1008, Washington, D.C., 1996.
[15] A. Rockett, J.S. Britt, T. Gillespie and C. Marshall, *Thin Solid Films*, 217 (2000) 212–217.
[16] X.H. Tan, S.L. Ye, B. Fan, K. Tang and X. Liu, *Appl. Opt.,* 49 (2010) 3071–3074.
[17] S. Puttnins, S. Levcenco, K. Schwarzburg, G. Benndorf, F. Daume, A. Rahm, A. Braun, M. Grundmann and T. Unold, *Sol. Energy Mater. Sol. Cells*, 119 (2013) 281–286.
[18] K. Granath, M. Bodega and L. Stolt, *Sol. Energy Mater. Sol. Cells*, 60 (2000) 279–293.
[19] M. Ruckh, D. Schmid, M. Kaiser, R. Schaffler, T. Walter and H.W. Schock, in *Proceedings of the 1st World Conference Photovoltaic Energy Conversion*, p. 156–159, Piscataway, 1994.
[20] P.M.P. Salomé, A. Hultqvist, V. Fjallstrom, M. Edoff, B. Aitken, K. Zhang, K. Fuller and C. Kosik Williams, IEEE J. of Photovolt, (2014) 1–6.
[21] M. Lammer, R. Kniese and M. Powalla, *Thin Solid Films*, 451-452 (2004) 175–178.

[22] S.L. Ye, X.H. Tan, M. Jiang, B. Fan, K. Tang and S. Zhuang, Appl. Opt., 49 (2010) 1662–1665.
[23] D. Rudmann, D. Brémaud, H. Zogg and A.N. Tiwari, J. Appl. Phys., 97 (2005) 084903.
24 D. Rudmann, D. Brémaud, A.F. da Cunha, G. Bilger, A. Strohm, M. Kaelin, H. Zogg and A.N. Tiwari, *Thin Solid Films*, 480-481 (2005) 55–60.
[25] C. Roger, G. Altamura, F. Emieux, O. Sicardy, F. Roux, R. Fillon, P. Faucherand, N. Karst, H. Fournier, L. Grenet, F. Ducroquet, A. Brioude and S. Perraud, *J. Renewable Sustainable Energy*, 6 (2014) 011405.
[26] R. Wuerz, A. Eicke, F. Kessler, P. Rogin and O. Yazdani-Assl, *Thin Solid Films*, 519 (2011) 7268–7271.
[27] J.H. Yun, K.H. Kim, M.S. Kim, B.T. Ahn, S.J. Ahn, J.C. Lee and K.H. Yoon. *Thin Solid Films*, 515 (2007) 5876–5879.
[28] P. Blösch, S. Nishiwaki, L. Kranz, C.M. Fella, F. Pianezzi, T. Jäger, C. Adelhelm, E. Franzke, S. Buecheler and A.N. Tiwari, *Sol. Energy Mater. Sol. Cells*, 124 (2014) 10–16.
[29] M. Lee, S.M. Lee, S. Jung, S. Ahn, J.S. Cho, J. Park, Y. Eh, J. Gwak, K. Shin, K. Yoon, Y.S. Cho, and J.H. Yun, *Appl. Surf. Sci*., 346 (2015) 562.
[30] M. Bodegärd, L. Stolt and J. Hedstrom in *12th European Photovoltaic Solar Energy Conference*, p. 1743–1746, 1994.
[31] A. Rockett, *Thin Solid Films*, 480-481 (2005) 2–7.
[32] D.W. Niles, M. Al-Jassim and K. Ramanathan, *J. Vac. Sci. Technol. A*, 17 (1999) 291–296.
[33] E. Cadel, N. Barreau, J. Kessler and P. Pareige, *Acta Mater*, 58 (2010):2634–2637.
[34] R. V. Forest (2015) '*Diffusion Of Sodium In Copper Indium Gallium Diselenide Based Materials'*, Ph.D. Dissertation, University of Delaware.
[35] J. H. Scofield, S. Asher, D. Albin, J. Tuttle, M. Contreras, D. W Niles, R. Reedy, A. Tennant and R. Noufi, in *Proceedings of the 1st IEEE World Conference on Photovoltaic Energy Conversion*, p. 164–167, Piscataway, 1994.
[36] J.-H. Yoon, S. Cho, W. M. Kim, J.-K. Park, Y.-J. Baik, T. S. Lee, T.-Y. Seong and J.-H. Jeong, *Sol. Energy Mater. Sol. Cells*, 95 (2011) 2959–2964.
[37] P. Bommersbach, L. Arzel, M. Tomassini, E. Gautron, C. Leyder, M. Urien, D. Dupuy and N. Barreau, *Prog. Photovolt. Res. Appl.,* 21 (2013) 332–343.
[38] J.-H. Yoon, T.-Y. Seong and J.-H. Jeong, *Prog. Photovolt. Res. Appl*., 21 (2013) 58–63.
[39] K. Granath, L. Stolt, M. Bodegård, A. Rockett and D. J. Schroeder, in *14th European Photovoltaic Solar Energy Conference*, p. 1278–1282, Barcelona, 1997.
[40] A. Rockett, M. Bodegård, K. Granathc and Lars Stolt, in *25th IEEE Photovoltaic Specialist Conference*, p. 985–987, Washington, D.C., 1996.
[41] H. A. Al-Thani, F. S. Hasoon, M. Young, S. Asher, J. Alleman, M. Al-Jassim and D. Williamson, in *Proceedings of the Twenty-Ninth IEEE Photovoltaic Specialists Conference*, p. 720–723, New Orleans, 2002.
[42] P.R. Subramanian, in *Binary Allow Phase Diagrams,* T.B. Massalski, editor, 2nd Edition, p. 2631–2633, ASM International, 1990.

[43] L. Assmann, J. C. Bernede, A. Drici, C. Amory, E. Halgand and M. Morsli, Appl. Surf. Sci., 246 (2005) 159–166.
[44] M. B. Zellner, R. W. Birkmire, E. Eser, W. N. Shafarman and J. G. Chen, Prog. Photovolt. Res. Appl., 11 (2003) 543–548.
[45] P. M. P. Salomé, V. Fjallstrom, A. Hultqvist, P. Szaniawski, U. Zimmermann and M. Edoff, *Prog. Photovolt. Res. App*., 22 (2013) 83–89.
[46] S. C. Srivastava and L. L. Seigle, Metall. Trans., 5 (1974) 49–52.
[47] J.C.M. Hwang and R.W. Balluffi, J. Appl. Phys., 50 (1979) 1339–1348.
[48] J. Palm, V. Probst, A. Brummer, W. Stetter, R. Tölle, T.P. Niesen, S. Visbeck, O. Hernandez, M. Wendl, H. Vogt, H. Calwer, B. Freienstein and F. Karg, *Thin Solid Films*, 431-432 (2003) 514–522.
[49] D Gupta. in *Diffusion Phenomena in Thin Films and Microelectronic Materials*, D. Gupta and P. S. Ho, editors, p. 44. Noyes Publications, Park Ridge, NJ, 1988.
[50] P. Arnoldy, J. C. M. de Jonge and J. A. Moulijn. *J. Phys. Chem*., 89 (1985) 4517–4526.
[51] M. Bodegärd, K. Granath, L. Stolt and A. Rockett, *Sol. Energy Mater. Sol. Cells*, 58 (1999) 199–208.
[52] T. Wada, N. Kohara, S. Nishiwaki and T. Negami, *Thin Solid Films*, 387 (2001) 118–122.
[53] R. V. Forest, E. Eser, B. E. McCandless, R. W. Birkmire and J. G. Chen, *AICHE Journal,* 60 (2014) 2365-2372.
[54] M. Contreras, B. Egaas, P. Dippo, J. Webb, J. Granata, K. Ramanathan, S. Asher, A. Swartzlander and R. Noufi, in *Proceedings of the 26th IEEE Photovoltaic Specialist Conference,* p. 359–362, Anaheim (1997).
[55] J. Granata and J. Sites, in *Proceedings of the 2nd World Conference on Photovoltaic Solar Energy Conversion*, p. 604-607, Vienna (1998),.
[56] J. Holz, F. Karg and H. Philipsborn, in *Proceedings of the 12th European Photovoltaic Solar Energy Conference*, p.1592-1505, Amsterdam, (1994).
[57] D. W. Niles, K. Ramanathan, F. Hasoon, R. Noufi, B. J. Tielsch and J. E. Fulghum, *J. Vac. Sci. Technol. A*, 15 (1997) 3044.
[58] S.-H. Wei, S. B. Zhang and A. Zunger, *J. Appl. Phys*., 85 (1999) 7214.
[59] X. Sun, F. Jiang and J. Feng, *Comp. Mater. Sci*. 47 (2009) 31.
[60] E. S. Mungan, S. Member, X. Wang and M.A. Alam, *IEEE J. Photovolt.* 3 (2013) 451.
[61] A. Urbaniak, M. Igalson, F. Pianezzi, S. Bücheler, A. Chirilă, P. Reinhard and A. Tiwari, *Sol. Energ. Mat. Sol. Cells,* 128 (2014) 52.
[62] D. Cahen and R. Noufi, *Appl. Phys. Lett*., 54 (1989) 558.
[63] L. Kronik, D. Cahen and H.-W. Schock, *Adv. Mater*., 10 (1998) 31.
[64] G. M. Hanket, C. P. Thompson, J. K. Larsen, E. Eser and W. N. Shafarman, in *Proceedings of the 38th IEEE Photovoltaic Specialist Conference*, p. 662-667, Austin (2012).
[65] M. Wagner, *Simulation of thermoelectric devices*, Ph.D. thesis, Technical University of Vienna, 2007.
[66] R. V. Forest, E. Eser, B. E. McCandless, J. G. Chen and R.W. Birkmire, in *Proceedings of the 40th IEEE Photovoltaic Specialists Conference*, Denver (2014).

[67] D. J. Schroeder and A. A. Rockett, *J. Appl. Phys*. 82 (1997) 4982.
[68] S. Sadewasser, T. Glatzel, S. Schuler, S. Nishiwaki, R. Kaigawa and M. Lux-Steiner, *Thin Solid Films,* 431-432 (2003) 257.
[69] A. Virtuani, E. Lotter, M. Powalla, U. Rau, J. H. Werner and M. Acciarri, *J. Appl. Phys.* 99 (2006) 014906.
[70] K. Chattopadhyay, I. Sanya, S. Chaudhuri and A. Pal, *Vacuum*, 42 (1991) 915.
[71] R. V Forest, K. Han, E. Eser, J. G. Chen and R. W. Birkmire, in *Proceedings of the 39th IEEE Photovoltaic Specialists Conference*, Tampa (2013).
[72] R. Schlesiger, C. Oberdorfer, R. Würz, G. Greiwe, P. Stender, M. Artmeier, P. Pelka, F. Spaleck and G. Schmitz, *Rev. Sci. Instrum.* 81 (2010) 043703.
[73] P.-P. Choi, O. Cojocaru-Mirédin, R. Wuerz and D. Raabe, *J. Appl. Phys,* 110 (2011) 124513.
[74] O. Cojocaru-Mirédin, P. P. Choi, D. Abou-Ras, S. S. Schmidt, R. Caballero and D. Raabe, *IEEE J. Photovolt.,* 1 (2011) 207.
[75] J. Keller, R. Schlesiger, I. Riedel, J. Parisi, G. Schmitz, A. Avellan and T. Dalibor, *Sol. Energy Mater. Sol. Cells,* 117 (2013) 592.
[76] A. Laemmle, R. Wuerz, T. Schwarz, O. Cojocaru-Mirédin, P.-P. Choi and M. Powalla, *J. Appl. Phys.,* 115 (2014) 154501.
[77] K. Gartsman, L. Chernyak, V. Lyahovitskaya, D. Cahen, V. Didik, V. Kozlovsky, R. Malkovich, E. Skoryatina and V. Usacheva, *J. Appl. Phys.* 82 (1997) 4282.
[78] L.G. Harrison. *Trans. Faraday Soc.* 57 (1961) 1191.
[79] H. Mehrer, *Diffusion in Solids*, Springer-Verlag, Berlin, (2007).
[80] L. E. Oikkonen, M. G. Ganchenkova, A. P. Seitsonen and R. M. Nieminen, *J. Appl. Phys.* 114 (2013) 083503.
[81] L. E. Oikkonen, M. G. Ganchenkova, A. P. Seitsonen and R. M. Nieminen, *J. Appl. Phys.*113 (2013) 133510.
[82] J. Pohl and K. Albe, *J. Appl. Phys.,* 108 (2010) 023509.
[83] J. Pohl, A. Klein and K. Albe, *Phys. Rev. B*., 84 (2011), 121201.
[84] F. C. Frank and D. Turnbull, *Phys. Rev.,*104 (1956) 617.
[85] N. A. Stolwijk, S. Obeidi, J. Bastek, R. Wuerz and A. Eicke, *Appl. Phys. Lett.* 96 (2010) 244101.
[86] K. Hiepko, J. Bastek, R. Schlesiger, G. Schmitz, R. Wuerz and N. A. Stolwijk, *Appl. Phys. Lett.,* 99 (2011) 234101.
[87] R. V. Forest, E. Eser, B. E. McCandless, J. G. Chen and R. W. Birkmire, *J. Appl. Phys.* 117 (2015) 115102.
[88] R. V. Forest, B. E. McCandless, X. He, A. A. Rockett, E. Eser, K. D. Dobson, R. W. Birkmire, (2015) submitted to *Adv. Mater*.
[89] A. Chirilă, P. Reinhard, F. Pianezzi, P. Bloesch, A. R. Uhl, C. Fella, L. Kranz, D. Keller, C. Gretener, H. Hagendorfer, D. Jaeger, R. Erni, S. Nishiwaki, S. Buecheler and A. N. Tiwari, *Nature Materials*, 12 (2013) 1107-1111.
[90] P. Jackson,' D. Hariskos, R. Wuerz, W. Wischmann and M. Powalla, *Physica Status Solidi*, 8 (2014) 219-222.